haematologica
Journal of the Ferrata Storti Foundation

Elevated levels of Ube2g1 in hematopoietic stem cells lead to segmental aging of the hematopoietic system

by Julian Niemann, Tanja Schuster, Vadim Sakk, Karin Soller, Andreas Brown, Sebastian Wiese, Karina Eiwen, Markus Hoenicka, Andreas Liebold, Moritz Oltmanns, Heiko Reichel, Medhanie A. Mulaw and Hartmut Geiger

Received: July 31, 2025.
Accepted: January 23, 2026.

Citation: Julian Niemann, Tanja Schuster, Vadim Sakk, Karin Soller, Andreas Brown, Sebastian Wiese, Karina Eiwen, Markus Hoenicka, Andreas Liebold, Moritz Oltmanns, Heiko Reichel, Medhanie A. Mulaw and Hartmut Geiger. Elevated levels of Ube2g1 in hematopoietic stem cells lead to segmental aging of the hematopoietic system.
Haematologica. 2026 Feb 5. doi: 10.3324/haematol.2025.288847 [Epub ahead of print]

Elevated levels of Ube2g1 in hematopoietic stem cells lead to segmental aging of the hematopoietic system

Julian Niemann[1], Tanja Schuster[1], Vadim Sakk[1], Karin Soller[1], Andreas Brown[1], Sebastian Wiese[2], Karina Eiwen[1], Markus Hoenicka[3], Andreas Liebold[3], Moritz Oltmanns[4], Heiko Reichel[4], Medhanie A. Mulaw[5], Hartmut Geiger[1]

[1]Institute of Molecular Medicine, Ulm University, Germany
[2]Core Unit Mass Spectrometry and Proteomics, Ulm University, Germany
[3]Department of Cardiothoracic and Vascular Surgery, University Hospital, 89081 Ulm, Germany
[4] Department of Orthopaedic Surgery, University Hospital, 89081, Ulm, Germany
[5]Single-Cell Sequencing Unit, Ulm University, Germany

Figures: 5 (Main), 7 (Supplementary)
Tables: 5 (Supplementary)
Words: 150/4000 (Abstract/Main)
Short Title: Elevated Ube2g1 induces segmental HSC aging
Key words: HSC, Aging, Ube2g1, Phosphorylation, Ubiquitination

Data sharing statement

The authors confirm that the data supporting the findings of this study are available within the article and its supplementary materials. Raw data are available under accession numbers **GSE303039** and **MSV000098473**.

Author contributions

J.N. Conceptualization, Data curation, Formal analysis, Investigation, Methodology, Project administration, Software, Supervision, Visualization, Writing – original draft, Writing – review and editing. **T.S.** Conceptualization, Data curation, Investigation, Software, Writing – review and editing. **V.S.**, **K.S.** Conceptualization, Investigation, Writing – review and editing. **A.B.** Conceptualization, Data curation, Formal analysis, Investigation, Writing – review and editing. **S.W.** Data curation, Formal analysis, Investigation, Resources, Visualization, Writing – review and editing. **K.E.** Conceptualization, Investigation, Methodology, Writing – review and editing. **M.H. and A.L.** Resources, Data curation. **M.O. and H.R**. Resources, Data curation, review and editing. **M.A.M.** Conceptualization, Data curation, Formal analysis, Investigation, Software, Resources, Visualization, Writing – review and editing. **H.G.** Conceptualization, Funding acquisition, Methodology, Project administration, Resources, Supervision, Writing – original draft, Writing – review and editing.

Corresponding Authors:
Julian Niemann, Institute of Molecular Medicine, Ulm University, Germany; E-Mail: julian.niemann@uni-ulm.de; Tel.: +49 731 50 26713
Prof. Dr. Hartmut Geiger; Institute of Molecular Medicine, Ulm University, Germany; E-Mail: hartmut.geiger@uni-ulm.de; Tel.: +49 731 50 26700

Acknowledgements
We thank the members of the Institute of Molecular Medicine for their valuable comments and discussions. We are also grateful to the Core Facility Cytometry at Ulm University for their support in performing experiments. Special thanks go to the Tierforschungszentrum at Ulm University for their assistance with mouse handling and housing.

Competing Interest
The authors declare no competing interests related to the publication of this study.

Funding
The work was supported by the Deutsche Forschungsgemeinschaft (DFG, German Research Foundation) SFB1074 and SFB1506 Aging@Interfaces, both to **H.G.**

Abstract

Aged hematopoietic stem cells (HSCs) show diminished capacity of self-renewal, skewed lineage output and compromised proteostasis. Ubiquitin proteasomal systems are critical for maintaining protein homeostasis. We show that the levels of Ube2g1, a E2 ubiquitin-conjugating enzyme likely involved in clonal selection of HSCs, was elevated in aged murine and human HSCs. We hypothesized that elevated levels of Ube2g1 causally contribute to hematopoietic system aging. Elevated levels of Ube2g1 in young murine HSCs resulted in increased myeloid-to-lymphoid ratio and reduced naïve T-cells, both known hematopoietic aging hallmarks. Interestingly, the ubiquitination function of Ube2g1 didn't primarily account for the observed phenotypes. Elevated levels of Ube2g1 affected global tyrosine phosphorylation, mediated through a Ube2g1-Shp2 axis, which correlated with impaired T-cell development and reduced HSC function. Our work identifies a novel connection between proteins involved in the regulation of ubiquitination and phosphorylation in HSCs that affect phenotypes linked to aging of HSCs.

Introduction

Hematopoietic stem cells (HSCs) are essential for maintaining a functional hematopoietic system throughout lifespan. The delicate balance between self-renewal and differentiation is critical for preserving HSC function[1,2]. As organisms age, HSCs undergo a functional decline, contributing to age-associated changes in the hematopoietic system[3–5]. The aging process in HSCs involves a complex network of intra- and extracellular mechanisms, one of which is changes in proteostasis, the equilibrium between protein formation and degradation[6,7]. HSCs maintain low protein synthesis rates and high translation accuracy, coupled with efficient protein degradation systems which are tightly regulated[8,9].

Proteostasis comprises three main components: protein translation, folding, and degradation[8,10]. Previous research has emphasized the importance of protein translation and folding in quiescent cells like HSCs[8,11,12]. The nature of the degradation network within HSC though has not been addressed in detail. A key player in protein degradation is the ubiquitin-proteasome system (UPS), which tags proteins with ubiquitin for subsequent degradation by the 26S proteasome[4,7,13]. During HSC aging, the efficiency of the UPS declines, leading to the accumulation of damaged and misfolded proteins in aggregates. The differential regulation of these aggregates between young and aged HSCs affects HSC function[14,15].

E2 enzymes mediate ubiquitin transfer between E1 activating enzymes and E3 ligases, contributing to the diversity of ubiquitination through target and E3 specificity[16,17]. Data supports a role for the E2 ubiquitin-conjugating enzyme Ube2g1 in clonal selection of HSCs upon aging. Ube2g1 is thought to primarily catalyse the addition of K48-linked ubiquitin chains, which typically signal for substrate degradation[18]. Ube2g1 has been further implicated in treatment resistance of multiple myeloma via self-establishment of K48-Ub chains, suggesting a complex role beyond supporting E3 ligases[18,19]. Recent studies demonstrated an involvement of Ube2g1 in TRAF7-mediated DBD degradation and a potential connection to 3'UTR shortening in T-cell development[20,21].

Based on our preliminary data, we hypothesized that Ube2g1 is involved in HSC aging. We show here that increased levels of Ube2g1 in murine and human HSCs confer segmental aging on young murine HSCs and altered protein phosphorylation patterns, which correlated with changes in Shp2. Elevated levels of Ube2g1 impaired aging-associated T-cell development and reduced the function of HSCs.

Methods

Mice

Young wildtype (WT) C57/BL6J mice (10-16 weeks, CD45.2^{+}) and aged RFP$^{ki/ki}$ mice (>80 weeks, CD45.2^{+}) were used for competitive transplantations. Isolated HSCs were transduced and transplanted into lethally irradiated (7+4 Gy) young B6.SJL-Ptprc^{a} Pepc^{b}/BoyJ recipient mice (12-16 weeks, CD45.1^{+}). For other experiments young (10-16 weeks, CD45.2^{+}) and aged WT C57/BL6J mice (>80 weeks, CD45.2^{+}) were used.

HSC Transduction

LT-HSCs (Lin^{-}, c-Kit^{+}, Sca-1^{+}, CD34^{-}, Flt3^{-}) (**Supplementary Table 1**) were sorted from lineage depleted LDBM using FACS sorting (BD, Aria III). For transduction, HSCs were incubated for 16 hours in mHSC medium (IMDM with 10% FBS, 1% Pen/Strep, 1% GlutaMAX, 100ng/mL SCF, TPO & G-CSF) with VPs at MOI 30.

Flow Cytometry

Spleen and thymus were forced through a 70 µm filter to retrieve single cells and red blood cell lysed (Biolegend) prior to flow analysis with a LSRFortessa (BD). (**Supplementary Table 1**).

Immunofluorescence

Young (Median age: 32.5 years) and aged human (71.0 years) CD34^{+} HSCs were cultured in hHSC medium (StemSpan SFEM with 100 ng/ml SCF, 50 ng/ml TPO and 100 ng/ml Flt3). For preparation of cells for IF we followed the protocol published by our group[22]. Antibodies are listed in **Supplementary Table 1.**

Proximity Ligation Assay (PLA)

After fixation and permeabilization[22], the Duolink Proximity Ligation Assay (Sigma-Aldrich) was used according to the manufacturer's instructions with the addition of a GFP counterstaining.

Production and titration of lentiviral particles

Viral particles (VPs) were generated using a Transfection Kit (Takara Bio). We used a GFP cassette that was inserted downstream of the ORF (Control, Ube2g1-OE, Ube2g1C90S -OE, shScrambled and shUbe2g1) with a TRTRPLE linker. Plasmids were transfected in 293T-LentiX cells (TakaraBio) and VPs harvested, concentrated by ultracentrifugation and titres determined[23].

Mass spectrometry

Digestion, elution and measurement as well as quantitative analysis and peptide identification with Andromeda were performed as previously described[24–26]. To identify Ube2g1interacting proteins, positive outliers found by Significance B testing[25] in addition to proteins with a log2 Ube2g1/ctrl ratio >2 were considered (**Supplementary Table 5**).

Ube2g1-OE^{C90S} generation

Data from Lu *et al.*[19] were used for the generation of the C90S mutated Ube2g1-OE plasmid. A site-directed mutagenesis kit (NEB) was used to introduce the base substitution (**Figure S4A**).

RNA-Sequencing

Transduced HSCs were sorted and processed according to the SMART Seq. v4 Ultra Low Input RNA Kit (Takara Bio). Libraries were prepared with the Nextera XT library Kit (Illumina). Raw data were processed, aligned and mapped as previously described[27,28]. For GoTerms analysis (**Supplementary Table 3**), DEG's from selected comparisons were used in GOrilla[29].

Ethical statement

Our research complies with all relevant ethical regulations and was performed in compliance with German Law for Welfare of Laboratory Animals approved by the Regierungspräsidium Tübingen and the Ethikkommission of Ulm University (IRB Approvals: 66/24, 392/16).

Graphical illustrations

Graphical schemes were generated with BioRender.com under an Academic Lab License.

Quantification and statistical analysis

The statistical tests used are mentioned in the respective figure legends. We performed multiple experiments with biological replicates to ensure data reproducibility.

Results

Expression of Ube2g1 is increased in aged murine HSC and aged human HSPCs.

A replication deficient retroviral insertional mutagenesis screen[30] identified, among others, elevated levels of Ube2g1, an E2 enzyme relevant for degradation specific K48-ubiquitination establishment, as a likely target for conferring aging-associated clonal advantages to HSCs[22,36] (**Figure S1A**). We therefore determined the level of Ube2g1 protein in young and aged murine HSCs by quantitative immunofluorescence imaging (QIF[22]). Aged

murine long-term HSCs (LT-HSCs; Lin^-, $Sca1^+$, $c\text{-}Kit^+$, $CD34^-$, $Flt3^-$) exhibited increased levels of Ube2g1 protein compared to young cells (**Figure 1A, B**). Levels of ubiquitin and lysine-48-linked ubiquitin (K48-Ub), proteins that are like Ube2g1 critical for protein degradation, showed a mild reduction in the case of overall ubiquitin (**Figure S1B, C**) while there was an increase in the level of K48-Ub (**Figure S1D, E**). K48-Ub primarily targets proteins towards proteasomal degradation. Elevated levels of K48-Ub have been also reported in age-related protein aggregation diseases[31–33]. Similarly to our findings in murine HSCs, the levels of both Ube2g1 and K48-Ub were also increased in aged human BM-derived $CD34^+$ HSPCs (donor >60 years) compared to HSCs from young donors <30 years, while levels of ubiquitin were not affected by aging (**Figure 1C, D; Figure S1F-I**). These findings are consistent with elevated levels of proteins marked for degradation in aged HSCs, while further experiments will be required to test for the overall flux of protein degradation in especially aged human HSC.

Elevated levels of Ube2g1 result in segmental premature aging of HSCs.

We next investigated the extent to which an elevated level of expression of Ube2g1 in young HSCs changes functional parameters in HSCs that are associated with aging. Competitive transplantation experiments of young and aged LT-HSCs transduced with an GFP-tagged Ube2g1 that conferred elevated levels of expression of Ube2g1 to HSCs (OE HSCs) (**Figure 1E; Figure S2A-D**) revealed a pronounced myeloid bias (myeloid cell frequency over lymphoid cell frequency) driven by OE HSCs in peripheral blood (PB) of the recipient mice. There was a three-fold increase of the myeloid bias in animals transplanted with OE young cells, which increased to 18-fold in recipients of OE aged HSCs when compared to the myeloid over lymphoid ratio in animals transplanted with HSCs transduced with a control virus (**Figure 1F**). The shift was due to a four-fold decrease in T-cells and a two-fold increase in myeloid cells in recipients of young OE HSCs, while animals transplanted with aged OE cells showed a six-fold reduction in T-cells and a 50% increase in myeloid cells in the PB compared to controls (**Figure 1G**). This myeloid shift was also present in the spleen, but not in the BM of the recipients (**Figure S2E-H**). Elevated levels of OE did not affect the frequency of young HSCs or the aging-associated increase of aged HSCs[3,34], as well as the frequency of young and aged myeloid progenitor cells in BM (**Figure S2I, J**).

Upon aging, there is a reduction in the frequency of naïve $CD8^+$ T-cells and an increase in the frequency of $CD8^+$ memory T-cells in spleen[28,35]. Recipients of young OE-HSCs already showed a substantial reduction in the frequency in naïve CD8-positive T-cells ($CD8^+$, $CD44^-$, $CD62L^+$) (**Figure 1H, I**), while they were completely absent in recipients of aged OE HSCs. Conversely, the frequency of central memory T-cells ($CD8^+$, $CD44^+$, $CD62L^+$) was increased

in the spleen of recipients that received either young or aged OE HSCs. The frequency of effector T-cells ($CD8^+$, $CD44^+$, $CD62L^-$) was not affected in OE-transplanted mice. Moreover, also the frequency of naïve (lower upon aging) and memory (elevated upon aging) $CD4^+$ T-cells cells in the spleen of animals transplanted with Ube2g1-OE HSCs mirrored the frequency of their $CD8^+$ counterparts in OE HSCs recipients (**Figure S2K**). Collectively, these findings support that elevated levels of Ube2g1 in HSCs can be causative for segmental aging-like differentiation phenotypes of HSCs.

We next investigated the extent to which a reduction of the expression of Ube2g1 in aged HSCs might reduce aging-associated phenotypes of aged HSCs. Competitive transplantation experiments of aged LT-HSCs transduced with an GFP-tagged shRNA against Ube2g1 that reduced elevated levels of expression in aged HSCs (KD HSCs) (**Figure S3A-D**) demonstrated that indeed, reduced levels of Ube2g1 resulted in a decreased myeloid bias compared to aged controls (**Figure S3E, F**), driven by a lower frequency of myeloid cells in combination with a modest increase of T- and B-cells in PB. Ube2g1-KD in aged HSCs did not affect the aging-associated reduction in naïve $CD8^+$ T-cells in spleen or myeloid bias reported for aged HSCs (**Figure S3G, H**). T/B- and myeloid cells in BM were similar to animals transplanted with aged control HSCs (**Figure S3I**), while the aging-associated increase in the frequency of HSC in aged BM was reduced in animals transplanted with aged Ube2g1-KD HSCs (**Figure S3J**). While these data support an overall causal role of an elevated level of Ube2g1 for conferring aging-associated phenotypes on HSCs, they also reveal that there is only a segmental set of phenotypes affected by Ube2g1.

The ubiquitination function of Ube2g1 is not required for conferring aging-associated phenotypes on HSCs

Lu et al. demonstrated, in large sets of experiments, that a C90S point mutation in Ube2g1 renders the ubiquitination function of Ube2g1 inactive, and that Ube2g1-C90S is not able to ubiquitinate target proteins[19]. We therefore performed competitive transplantation experiments with HSCs that were transduced with Ube2g1-C90S-OE to test for the role of the ubiquitination function of Ube2g1 for conferring the aging-associated phenotypes. (**Figure 2A, B; Figure S4A-D**). Unexpectedly, Ube2g1-C90S-OE didn't alter the segmental aging phenotype conferred by the elevated level of Ube2g1. Recipients receiving Ube2g1-C90S-OE HSCs still exhibited a 12-fold increase in the myeloid-to-lymphoid cell ratio in peripheral blood due to a reduction in T-cells and an increase in myeloid cells (**Figure 2C, D**). Also, the reduction in frequency of naïve $CD8^+$ T-cells and an increase in the frequency of effector T-cell (**Figure 2E**) as well as a shift of the myeloid-to-lymphoid ratio in the spleen (**Figure S4E, F**) conferred by Ube2g1-OE was not affected by the point mutation. Ube2g1-

C90S HSCs mirrored the function of Ube2g1-OE HSCs also with respect to the frequency of mature T-, B-, and myeloid cells as well as LT-HSCs and myeloid progenitor populations in BM (**Figure S4G-I**). Collectively, these findings imply that enzymatic function “ubiquitination of target substrates bound to an E3 enzyme” of Ube2g1 is likely not the main mechanistic driver conferring aging-like phenotypes on Ube2g1-OE HSCs.

Elevated levels of Ube2g1 results in changes in phosphorylation and immune system pathways.

We next employed RNA sequencing approaches on Ube2g1-OE HSCs to obtain insights into likely molecular mechanisms on the action of Ube2g1 (**Figure 3A**). Analysis of the sample distribution using a 2-dimensional PCA identified a greater heterogeneity among young Ube2g1-OE HSCs compared to aged Ube2g1-OE HSCs (**Figure 3B**). While there was an overall large number of differentially expressed genes (DEGs) between young and aged cells, unsupervised clustering of differentially expressed genes revealed a strong shift in the transcriptional landscape of young Ube2g1-OE HSPCs, while a more muted difference was observed for the transcriptional pattern of aged Ube2g1-OE HSPCs (**Figure 3C**). Clustering of the DEGs into functionals groups via Gene Ontology (GO) analyses revealed terms associated with protein phosphorylation among the top hits, along with terms related to cytokine production (**Figure 3D; Supplementary Table 3**). So far, Ube2g1 has not been associated with a role in the regulation of protein phosphorylation. To obtain additional information with respect to the phosphorylation-related terms, these DEG’s were plotted on a volcano plot. Additional analyses revealed a strong association of GOs in Ube2g1-OE HSPCs with TCR and MAPK signalling, represented by Zap70 and Ptpn11 (Shp2) expression (**Figure 3E; Supplementary Table 4**).

In parallel co-immunoprecipitation (Co-IP) and mass spectrometry approaches, we identified potential protein interaction partners of Ube2g1 (**Figure 3F, G; Supplementary Table 5**). We identified Uba52, an E1 ubiquitin donor, as a likely prime Ube2g1-OE partner (**Figure S5A, B**). Unexpectedly, Shp2 (a phosphatase), for which we observed increased expression in young Ube2g1-OE compared to control HSCs, emerged again as a potential interactor. Furthermore, we identified a cluster of heat shock proteins (Hspa1a, Hspa2, Hspa4, Hspa8) as potential binding partners. We therefore also investigated a likely role of heat shock factor 1 (Hsf1), a regulator of heat shock protein expression, in Ube2g1-OE HSCs. Young Ube2g1-OE HSCs showed reduced levels of Hsf1, which aligns with an age-associated decrease in Hsf1 expression in HSPCs (**Figure S5C, D**). We made use of proximity ligation assays (PLA) to confirm key interactors of Ube2g1 in HSCs. In physiological control conditions, we found Ube2g1 to be in close proximity (less than 40 nm) to both Creb3, a leucine zipper DNA binding protein, and Uba52. The average frequency of such a very close interaction of

Ube2g1 with either Creb3 or Uba52 was increased in Ube2g1-OE HSCs, suggesting increased levels of interaction upon an increase in protein (**Figure S5E-K**), further supporting direct interaction of these proteins.

Elevated levels of Ube2g1 reduce global tyrosine phosphorylation and the level of Shp2 phosphatase

As the RNA-Sequencing as well as the Co-IP analyses showed changes in general protein phosphorylation in response to elevated levels of Ube2g1 in HSCs, we determined the level of protein phosphorylation as well as the level of Shp2 expression in Ube2g1-OE HSCs (**Figure 4A; Figure S6A**). In aged HSCs, the level of tyrosine-specific phosphorylation (pTyr) was decreased to 60% compared to young HSCs. Ube2g1-OE in young HSCs reduced the level of pTyr to that of aged HSCs (**Figure 4B, C**). Interestingly, there was a high level of correlation for the localization of pTyr and Ube2g1 within HSCs, with Pearson correlation coefficients (PCC) of approximately 0.7 across all samples (**Figure 4D**).

In contrast to increased expression of Shp2 in our transcriptomic data, we observed a reduction in Shp2 protein levels in young Ube2g1-OE HSCs (**Figure 4E, F**). Mirroring Ube2g1 and pTyr, the level of co-localization (PCC) between Ube2g1 and Shp2 was high across all samples, suggesting an elevated likelihood of protein interactions (**Figure 4G**). We also determined the level of pTyr and Shp2 in Ube2g1-KD and Ube2g1-C90S-OE in comparison to their respective control. There was an overall reduced level for both, pTyr and Shp2, and their levels were similar to the levels observed in Ube2g1-OE and aged HSCs (**Figure S6B-E**). Inhibition of Shp2 by a specific pharmacological inhibitor (SHP009) resulted, as anticipated, in reduced levels of the active form of Shp2 (phosphorylated at tyrosine 542, **Figure 4H**) and in then elevated levels of pTyr in HSCs (**Figure 4I**). Interestingly, inhibition of Shp2 in Ube2g1-OE HSCs, while further reducing the level of Shp2-pY452, did not affect the level of pTyr in HSCs. To test for a direct (less than 40 nm) Ube2g1-Shp2 interaction, PLAs were performed. Ube2g1 interacts with Shp2 in young and old control HSCs. The average interactions per cell did increase 2-fold in Ube2g1-OE HSCs. These data further confirmed results from our mass spectrometry and RNA-sequencing analyses (**Figure 4J-L**). In summary, the data support that elevated levels of Ube2g1 reduce the amount of pTyr in HSCs, while they also reduce levels of Shp2 and that Ube2g1 can directly interact with Shp2. Overall, the data thus suggest a complex relationship between Ube2g1, Shp2 and levels of pTyr in HSCs, which might be explained by a model in which Ube2g1 serves as a protein interaction platform to balance active forms of proteins involved in the regulation of overall protein phosphorylation.

Elevated levels of Ube2g1 result in attenuated T-cell development in the thymus and increased exhaustion in released peripheral T-cells.

Shp2 and protein phosphorylation are, among others, known regulators of T-cell development, and Ube2g1-OE in HSCs strongly affected the level of mature T-cells in the periphery (**Figure 1G**). Ube2g1 might therefore affect also thymic T-cell development (**Figure 5A**). T-cell development in the thymus involves three key stages: double-negative (DN1-DN4; $CD4^-CD8^-$), double-positive (DP; $CD4^+CD8^+$), and single-positive (SP; $CD4^+$ or $CD8^+$, $CD3^+$) cells (**Figure 5B**). In concordance with a general age-related increase in frequency, the percentage of DP thymocytes was also significantly increased in mice transplanted with young OE HSCs. The data further suggested a partial impairment in the DP-to-SP transition and an accelerated DN1-to-DN2 progression, with an additional potential blockage of OE cells in DN2 and DN3 (**Figure 5C-E**). Elevated levels of Ube2g1 therefore likely affect multiple transition points in thymic T-cell development. In addition to the relative changes within the populations, we observed a reduction in each cell type analysed in recipients of young OE HSCs, along with a reduction of cell populations in recipients transplanted with aged control HSCs (**Figure S7A, B**). To investigate additional changes in maturation of T-cells downstream of the thymus, we also assessed the level of exhaustion of T-cells (Expression of Tim-3 and PD-1) (**Figure 5F**). Recipients of Ube2g1 OE HSCs exhibited an elevated frequency of $CD8^+$ Tim-3^+ positive cells and a marked enrichment of Tim-3^+/PD-1^+ double-positive cells in spleen similar to cells from spleen from aged mice, which implies increased levels of T-cell exhaustion. The frequency of PD-1^+ T-cells though, although elevated in aged HSCs, was not affected by Ube2g1 OE (**Figure 5G**). Exhaustion in $CD4^+$ T-cells mirrored the level of exhaustion seen in CD8-positive splenocytes (**Figures S7C**). To investigate the extent of Shp2 involvement in this T-cell deficiency, *in vitro* CD8 T-cell activation/proliferation assay (activation by anti-CD3/CD28) were performed (**Figure S7D**). $CD8^+$ Ube2g1-OE T-cells showed a lower extent of activation in the activation/ expansion assays when compared to c T-cells (**Figure S7E-G**). There were reduced levels of active Shp2 (Shp2-pY542) in Ube2g1-OE T-cells, accompanied by increased levels of pTyr in both young Ube2g1-OE and old control T-cells (**Figure S7H, I**). Ube2g1 therefore affects T-cells at multiple steps along their differentiation, maturation, activation and exhaustion trajectory. This implies a more general role for Ube2g1 in T-cell differentiation and function, which is consistent with a role of Ube2g1 in regulating more general patterns of phosphorylation.

Discussion

Several E2 conjugation enzymes, which mediate the transfer of ubiquitin to substrates bound to E3 ligases which then mark proteins for degradation, have been shown to play a role in

stem cell biology[7,36,37]. Ube2g1 belongs to the group of E2 conjugation enzymes. Our data identified elevated levels of Ube2g1 along with K48-Ub in aged murine and human HSCs. We demonstrate that increased Ube2g1 levels in murine HSCs cause segmental pre-mature aging of the hematopoietic system. The following hallmarks of aging were recapitulated in animals transplanted with young Ube2g1-OE HSCs: Stem cell exhaustion, immune cell disbalance, myeloid skewing and proteostasis loss. Reduction of the aging-associated increase in Ube2g1 in aged murine HSCs attenuates myeloid skewing by affecting both myeloid and lymphoid differentiation. There is a reduction of naïve T-cells concomitant with an increase in exhausted peripheral T-cells in response to elevated levels of Ube2g1 in HSCs. Elevated levels of Ube2g1 resulted in elevated levels of exhaustion markers like Tim-3 on peripheral T-cells. Elevated levels of Tim-3 expression/exhaustion were shown to be linked to myelodysplastic HSCs and leukemic stem cells (LSC)[38,39], which might link Ube2g1 to an enhanced clonal selection of HSCs. However, we did not observe MDS-related morphological or cytological changes driven by Ube2g1-OE HSCs up to 24 weeks post-transplantation in our recipients, possibly due to insufficient exposure time or lack of additional stressors. Additionally, we found Ube2g1-OE T-cells to be less activated compared to controls upon in vitro expansion/activation culture, with a decrease in the level of active Shp2 (pY542) and an increase in the level of pTyr, supporting a role for a Ube2g1-OE-Shp2-pTyr axis in T-cell activation. Likely due to the overall low number of T- cells within the bone marrow, premature aging was less prominent among BM-cells compared to spleen and blood. These data also imply that lymphocytes derived from OE HSCs may be less capable of mounting an adequate immune response, which will be an interesting hypothesis to test in future experiments.

Surprisingly, our data suggest that the ubiquitin-conjugating activity of Ube2g1 is likely not the central underlying mechanisms for conferring the aging-associated phenotypes, while transcriptome analyses identified several E3 ligases (Cbl, Traf6, Fbxw7, Hectd1, Hectd2) as upregulated in response to Ube2g1-OE. Although the pulldown-data in NIH3T3 cells did not indicate direct protein-protein interactions with any of these E3 ligases, indirect interactions via shared degradation substrates or then altered phosphorylation signalling remain an alternative mode of interaction. This might imply that distinct levels of Ube2g1 affect the regulation of the general ubiquitin-proteasome system in HSCs, which would be consistent with the elevated levels of K48-Ub found in aged murine and human HSCs. Whether elevated levels of K48-Ub are mechanistically linked to conferring segmental aging phenotypes remains to be determined.

We identified a cluster of heat shock proteins, including Hspa8, as potential Ube2g1 interactors. Notably, the level of Hsf1, a key regulator of the heat shock response and an important regulator of for HSC function[11], was also reduced in Ube2g1-OE HSCs, implying that the proteostasis might also be affected by Ube2g1 in HSCs.

We show here both a reduction of tyrosine phosphorylation and total levels of Shp2 in aged and Ube2g1-OE HSCs. Shp2 is a phosphatase and thus negatively regulates tyrosine phosphorylation residues. Dysfunctional Shp2 signalling is known to play a role in HSC biology and T-cell development[40,41]. Further, impaired tyrosine phosphorylation strongly correlates with dysfunctional T-cell development and T-cell receptor (TCR) signaling, due to changes in MAPK/ERK or JAK/STAT signaling pathways downstream of the TCR[42,43]. The observed loss of tyrosine phosphorylation might lead to disrupted initiation and propagation of TCR signaling, indispensable for T-cell development in hematopoiesis[44,45]. Additionally, loss of tyrosine phosphorylation inactivates kinases like Zap70 and Lck, proven to be vital for thymic T-cell selection[46,47]. Dysregulation of such pathways in aging/response to Ube2g1-OE might contribute to altered T-cell maturation and the more exhausted adaptive immune system. This would initially imply that Shp2 is likely not directly linked to the changes in phosphorylation observed. On the other hand, we observed increased levels of active Shp2 (pY542), which is then consistent with a lower overall tyrosine phosphorylation in HSCs.

Our proteomic data further identified Shp2 as a potential direct Ube2g1 interactor, which is supported by co-localization and interactions below 40 nm in HSCs, linking Ube2g1 to the regulation of tyrosine phosphorylation. While inhibition of Shp2 activity resulted, as expected, to increased levels of phosphorylated proteins in young HSCs, it did not affect pTyr levels in Ube2g1-OE HSCs. Possibly Ube2g1 can act as a signaling platform that balances Shp2 signaling and by this means contribute to the level of protein phosphorylation. In such a model, the proper propagation of the signal of Shp2 is impaired if Ube2g1 is disturbed. As we also report a direct interaction of Ube2g1 with Creb3 and Uba52 in HSCs, Ube2g1 might form a broader mechanistic/physical protein platform, a hypothesis that will need to be tested in future experiments.

In summary, our findings identify Ube2g1 as a regulator of age-associated changes in HSC biology, particularly affecting T-cell development and exhaustion but also myeloid differentiation driven by HSCs, likely via mechanisms that involve phosphorylation driven mechanisms, Shp2-mediated pathways, proteostasis and ubiquitin signalling pathways.

References

1. Laurenti E, Göttgens B. From haematopoietic stem cells to complex differentiation landscapes. Nature. 2018;553(7689):418-426.
2. Pinho S, Frenette PS. Haematopoietic stem cell activity and interactions with the niche. Nat Rev Mol Cell Biol. 2019;20(5):303-320.
3. Geiger H, De Haan G, Carolina Florian M. The ageing haematopoietic stem cell compartment. Nat Rev Immunol. 2013;13(5):376-389.
4. Mejia-Ramirez E, Florian MC. Understanding intrinsic hematopoietic stem cell aging. Haematologica. 2020;105(1):22-37.
5. de Haan G, Lazare SS. Aging of hematopoietic stem cells. Blood. 2018;131(5):479-487.
6. López-Otín C, Blasco MA, Partridge L, Serrano M, Kroemer G. Hallmarks of aging: An expanding universe. Cell. 2023;186(2):243-278.
7. Moran-Crusio K, Reavie LB, Aifantis I. Regulation of hematopoietic stem cell fate by the ubiquitin proteasome system. Trends Immunol. 2012;33(7):357-363.
8. Signer RAJ, Magee JA, Salic A, Morrison SJ. Haematopoietic stem cells require a highly regulated protein synthesis rate. Nature. 2014;509(7498):49-54.
9. Noormohammadi A, Calculli G, Gutierrez-Garcia R, Khodakarami A, Koyuncu S, Vilchez D. Mechanisms of protein homeostasis (proteostasis) maintain stem cell identity in mammalian pluripotent stem cells. Cell Mol Life Sci. 2018;75(2):275-290.
10. Pickart CM, Eddins MJ. Ubiquitin: Structures, functions, mechanisms. Biochim Biophys Acta Mol Cell Res. 2004;1695(1-3):55-72.
11. Kruta M, Sunshine MJ, Chua BA, et al. Hsf1 promotes hematopoietic stem cell fitness and proteostasis in response to ex vivo culture stress and aging. Cell Stem Cell. 2021;28(11):1950-1965.e6.
12. Liu B, Zhang X, Zhou Y, et al. USP4 regulates ribosome biogenesis and protein synthesis for hematopoietic stem cell regeneration and leukemia progression. Leukemia. 2024;38(11):2466-2478.
13. Chua BA, Signer RAJ. Hematopoietic stem cell regulation by the proteostasis network. Curr Opin Hematol. 2020;27(4):254-263.
14. Dong Q, Xiu Y, Wang Y, et al. HSF1 is a driver of leukemia stem cell self-renewal in acute myeloid leukemia. Nat Commun. 2022;13(1):1-17.
15. Chua BA, Lennan CJ, Sunshine MJ, et al. Hematopoietic stem cells preferentially traffic misfolded proteins to aggresomes and depend on aggrephagy to maintain protein homeostasis. Cell Stem Cell. 2023;30(4):460-472.
16. Ryu K-S, Choi Y-S, Ko J, et al. Direct characterization of E2-dependent target specificity and processivity using an artificial p27-linker-E2 ubiquitination system. BMP Rep. 2008;41(12):852-857.
17. Stewart MD, Ritterhoff T, Klevit RE, Brzovic PS. E2 enzymes: More than just middle men. Cell Res. 2016;26(4):423-440.
18. Choi YS, Lee YJ, Lee SY, et al. Differential ubiquitin binding by the acidic loops of Ube2g1 and Ube2r1 enzymes distinguishes their Lys-48-ubiquitylation activities. J Biol Chem. 2015;290(4):2251-2263.
19. Lu G, Weng S, Matyskiela M, et al. UBE2G1 governs the destruction of cereblon neomorphic substrates. Elife. 2018:7:e40958.
20. Masuda S, Kurabayashi N, Nunokawa R, et al. TRAF7 determines circadian period through ubiquitination and degradation of DBP. Commun Biol. 2024;7(1):1-12.
21. Qiang J, Yu S, Li J, et al. Single-cell landscape of alternative polyadenylation in human lymphoid hematopoiesis. J Mol Cell Biol. 2024;16(7):1-16.
22. Schuster T, Amoah A, Vollmer A, et al. Quantitative determination of the spatial distribution of components in single cells with CellDetail. Nat Commun. 2024;15(1):1-13.
23. Brown LY, Dong W, Kantor B. An Improved Protocol for the Production of Lentiviral Vectors. STAR Protoc. 2020;1(3):100152.

24. Hecht M, Rösler R, Wiese S, Johnsson N, Gronemeyer T. An interaction network of the human SEPT9 established by quantitative mass spectrometry. G3 (Bethesda). 2019;9(6):1869-1880.
25. Cox J, Mann M. MaxQuant enables high peptide identification rates, individualized p.p.b.-range mass accuracies and proteome-wide protein quantification. Nat Biotechnol. 2008;26(12):1367-1372.
26. Cox J, Neuhauser N, Michalski A, Scheltema RA, Olsen J V, Mann M. Andromeda: A peptide search engine integrated into the MaxQuant environment. J Proteome Res. 2011;10(4):1794-1805.
27. Florian MC, Klose M, Sacma M, et al. Aging alters the epigenetic asymmetry of HSC division. PLoS Biol. 2018;16(9):1-35.
28. Leins H, Mulaw M, Eiwen K, et al. Aged murine hematopoietic stem cells drive aging-associated immune remodeling. Blood. 2018;132(6):565-576.
29. Eden E, Navon R, Steinfeld I, Lipson D, Yakhini Z. GOrilla: a tool for discovery and visualization of enriched GO terms in ranked gene lists. BMC Bioinformatics. 2009;10(1):1-7.
30. Kustikova O, Fehse B, Modlich U, et al. Clonal Dominance of Hematopoietic Stem Cells Triggered by Retroviral Gene Marking. Science. 2005;308(5725):1171-1174.
31. Ciechanover A, Kwon YT. Degradation of misfolded proteins in neurodegenerative diseases: therapeutic targets and strategies. Exp Mol Med. 2015;47(3):1-16.
32. David DC, Ollikainen N, Trinidad JC, Cary MP, Burlingame AL, Kenyon C. Widespread protein aggregation as an inherent part of aging in C. elegans. PLoS Biol. 2010;8(8):47-48.
33. Cuanalo-Contreras K, Schulz J, Mukherjee A, Park K-W, Armijo E, Soto C. Extensive accumulation of misfolded protein aggregates during natural aging and senescence. Front Aging Neurosci. 2023;14(11):1-15.
34. Guidi N, Marka G, Sakk V, Zheng Y, Florian MC, Geiger H. An aged bone marrow niche restrains rejuvenated hematopoietic stem cells. Stem Cells. 2021;39(8):1101-1106.
35. Nikolich-Žugich J. Aging of the T Cell Compartment in Mice and Humans: From No Naive Expectations to Foggy Memories. J Immunol. 2014;193(6):2622-2629.
36. Fatima A, Irmak D, Noormohammadi A, et al. The ubiquitin-conjugating enzyme UBE2K determines neurogenic potential through histone H3 in human embryonic stem cells. Commun Biol. 2020;3(1):1-19.
37. Zhan Q, Wang J, Zhang H, Zhang L. E3 ubiquitin ligase on the biological properties of hematopoietic stem cell. J Mol Med. 2023;101(5):543-556.
38. Tao J-L, Li L-J, Fu R, et al. Elevated TIM3+ hematopoietic stem cells in untreated myelodysplastic syndrome displayed aberrant differentiation, overproliferation and decreased apoptosis. Leuk Res. 2014;38(6):714-721.
39. Kikushige Y, Shima T, Takayanagi SI, et al. TIM-3 is a promising target to selectively kill acute myeloid leukemia stem cells. Cell Stem Cell. 2010;7(6):708-717.
40. Zhu HH, Ji K, Alderson N, et al. Kit-Shp2-Kit signaling acts to maintain a functional hematopoietic stem and progenitor cell pool. Blood. 2011;117(20):5350-5361.
41. Solman M, Blokzijl-Franke S, Piques F, et al. Inflammatory response in hematopoietic stem and progenitor cells triggered by activating SHP2 mutations evokes blood defects. Elife. 2022;11(e):73040.
42. Liu X, Qu C-K. Protein Tyrosine Phosphatase SHP-2 (PTPN11) in Hematopoiesis and Leukemogenesis. J Signal Transduct. 2011:2011:195239.
43. Williams MJ, Wang X, Bastos HP, et al. Maintenance of hematopoietic stem cells by tyrosine-unphosphorylated STAT5 and JAK inhibition. Blood Adv. 2025;9(2):291-309.
44. Shah K, Al-Haidari A, Sun J, Kazi JU. T cell receptor (TCR) signaling in health and disease. Signal Transduct Target Ther. 2021;6(1):1-26.
45. Stanford SM, Rapini N, Bottini N. Regulation of TCR signalling by tyrosine phosphatases: From immune homeostasis to autoimmunity. Immunology. 2012;137(1):1-19.

46. Castro-Sanchez P, Teagle AR, Prade S, Zamoyska R. Modulation of TCR Signaling by Tyrosine Phosphatases: From Autoimmunity to Immunotherapy. Front Cell Dev Biol. 2020:8:608747.
47. Hwang JR, Byeon Y, Kim D, Park SG. Recent insights of T cell receptor-mediated signaling pathways for T cell activation and development. Exp Mol Med. 2020;52(5):750-761.
48. Schmittgen TD, Livak KJ. Analyzing real-time PCR data by the comparative CT method. Nat Protoc. 2008;3(6):1101-1108.
49. Peach M, Marsh N, Miskiewicz EI, MacPhee DJ. Solubilization of Proteins: The Importance of Lysis Buffer Choice. Methods Mol Biol. 2015:1312:49-60.

Main Figure Legends

Figure 1: Elevated levels of Ube2g1 result in segmental premature aging of HSCs
A) Representative IF-pictures from young (12-16 weeks, WT) and aged (>80 weeks, WT) murine hematopoietic stem cells (HSCs) stained for Ube2g1 (red) and DAPI (blue), Scalebar = 5µm. **B)** Relative (log2 transformed) intensity of Ube2g1 in young and old murine HSCs (n = 7-11, biological repeats equal to an average of 83/155 (young/old) cells per replicate). **C)** Representative IF-pictures of human $CD34^+$ HSPCs from young (25-33 years donors; Mean = 30y) and old (55-80 years; Mean = 68y) donors stained for Ube2g1 (red) and DAPI (blue), Scalebar = 5µm. **D)** Relative (log2 transformed) intensity of Ube2g1 in young and old human $CD34^+$ HSPCs (n = 4-7, biological repeats equal to an average of 191/166 (young/old) cells per replicate). **E)** Schematic of the experimental set-up of the competitive transplantation experiment, using sorted HSCs from young (12-16 weeks, WT) and aged (>80 weeks, $AcRFP^+$) donor mice ($CD45.2^+$). HSCs were genetically engineered and transplanted alongside 5 $x10^4$ $CD45.1^+$ BM cells into lethally irradiated recipient mice ($CD45.1^+$). **F)** Ratio of the percentage of donor-derived (GFP^+) myeloid ($Gr\text{-}1^+/CD11^+$) over lymphoid ($CD3e^+$, $CD19^+$) cells in peripheral blood (PB) 24 weeks post-transplantation (n = 16-19, four independent experiment repeats). **G)** Percentage of donor-derived (GFP^+) T-cells ($CD3e^+$), B-cells ($CD19^+$) and myeloid cells ($Gr\text{-}1^+/CD11^+$) in PB 24 weeks post-transplantation (n = 17-19, four independent experiment repeats). **H)** Representative flow cytometry plots showing splenocytes gated for young and aged naïve ($CD62L^{dim}$, $CD44^-$), effector (EM; $CD62L^-$, $CD44^+$) and central memory cells (CM; $CD62L^+$, $CD44^+$) in animals transplanted with HSCs transduced with Ube2g1-OE or control virus. **I)** Percentage of donor-derived (GFP^+) naïve, CM and EM $CD8^+$ T-cells in the spleen 24 weeks post-transplantation (n = 17-19, four independent experiment repeats). Data show individual biological replicates with each replicate as mean ± SEM (B, D) or mean ± SD (F, G, I) from four independent repeats for mouse experiments. Data were assessed by a One sample t test against a value of 0 for young control (B, D) or by One-Way ANOVA or Kruskal-Wallis test depending on normality (F, G, I). *p < 0.05, **p < 0.01, ***p < 0.001, ****p < 0.0001.

Figure 2: The ubiquitination function of Ube2g1 is not required for conferring aging-associated phenotypes on HSCs
A) Schematic of the 3D structure of Ube2g1 with cysteine at position 90 highlighted within the active site of the enzyme. The substitution of cysteine with serine (C90S) in the active pocket leads to enzymatic inhibition of the UBC domain. **B)** Schematic of the experimental set-up of the competitive transplantation experiment, using sorted HSCs from young (12-16 weeks, WT) and aged (>80 weeks, $AcRFP^+$) donor mice ($CD45.2^+$). HSCs were genetically

engineered and transplanted alongside 5 x10^4 CD45.1^+ BM cells into lethally irradiated recipient mice (CD45.1^+). **C)** Percentage of donor-derived (GFP$^+$) T-cells (CD3e$^+$), B-cells (CD19$^+$) and myeloid cells (Gr-1^+/CD11^+) in PB 24 weeks post-transplantation (n = 5-6). **D)** Ratio of percentage of donor-derived (GFP$^+$) myeloid over lymphoid cells in PB 24 weeks post-transplantation (n = 5-6). **E)** Percentage of donor-derived (GFP$^+$) naïve, CM and EM CD8$^+$ T-cells in the spleen 24 weeks post-transplantation (n = 5-6). Data show individual biological replicates as mean ± SD. Data were assessed by One-Way ANOVA or Kruskal-Wallis test depending on normality (C-E). *p < 0.05, ***p < 0.001, ****p < 0.0001.

Figure 3: Elevated levels of Ube2g1 result in changes in phosphorylation and immune system pathways

A) Schematic of the workflow for RNA-Sequencing sample preparation. HSCs from young (12-16 weeks, wildtype) and aged (>80 weeks, wildtype) mice were genetically engineered and then sorted for GFP$^+$. The resulting cells were used for library preparation prior to RNA-Sequencing. **B)** Principal component analysis (PCA) (n = 4 biological replicates per condition). **C)** Heatmap comparing young and old control or Ube2g1-OE for differentially expressed genes (DEG's) between groups. Rows represent fold-change between different conditions and columns individual samples. Samples are subclustered according to similarities as depicted on the bottom of the heatmap and indicated as colours and black bars. On the left, depiction of gene clusters according to subclusters from the DEG analysis. On top of the heatmap, depiction of a phylogenetic tree for sample similarity depending on DEG's. **D)** Gene set enrichment analysis (GSEA) for the comparison of DEG's between the samples young with OE and control. All resulting gene ontologies (GO) were depicted. Colour indicates p-value and size of the circle gene counts. **E)** Comparison of significant DEG's between young OE and control. Top genes associated with the terms found in the GSEA are highlighted. **F)** Schematic of the workflow for immunoprecipitation (IP) followed by mass spectrometry for NIH/3T3 cells stably transduced with control or Ube2g1-OE. **G)** Proteins found in the comparison between NIH/3T3 cells with Ube2g1-OE and control after IP. Proteins that show significant differential presence are highlighted as red dots.

Figure 4: Reduction in global tyrosine phosphorylation and Shp2 phosphatase possibly through direct interaction

A) Schematic of the workflow for immunofluorescence preparation of transduced HSCs from young (12-16 weeks, wildtype) and aged (>80 weeks, wildtype) mice. **B)** Representative IF-pictures from young and old control and young Ube2g1-OE transduced murine HSCs stained for global tyrosine phosphorylation (red), GFP (green) and DAPI (blue), Scalebar = 5µm. **C)** Relative (log2 transformed) intensity of pTyr in young and old control and young

Ube2g1-OE transduced murine HSCs (n = 8-12, biological repeats equal to an average of 126/123 and 145/158 (young control/OE, old control/OE) cells per replicate). **D)** Pearson Correlation Coefficient (PCC) of pTyr and Ube2g1 in young and old control and young Ube2g1-OE transduced murine HSCs (n = 4-8) **E)** Representative IF-pictures from young and old control and young Ube2g1-OE transduced murine HSCs stained for Shp2 (red), GFP and DAPI, Scalebar = 5µm. **F)** Relative (log2 transformed) intensity of Shp2 in young and old control and young Ube2g1-OE transduced murine HSCs (n = 7-8, biological repeats equal to an average of 135/157 and 174/166 (young control/OE, old control/OE) cells per replicate). **G)** PCC of Shp2 and Ube2g1 in young and old control and young Ube2g1-OE transduced murine HSCs (n = 3). **H)** Average intensity of Shp2-pY542 in young control and Ube2g1-OE HSCs either untreated or treated with 100µM SHP009 for 15 minutes (n = 246-364 cells from 4 biological repeats). **I)** Average intensity of pTyr in young control and Ube2g1-OE HSCs either untreated or treated with 100µM SHP009 for 15 minutes (n = 245-341 cells from 4 biological repeats). **J)** Representative IF-pictures from young and old control and young Ube2g1-OE murine HSCs showing PLA signals (Shp2 and Ube2g1) and staining for GFP (transduced cells) and DAPI (nucleus). White arrows indicate PLA interactions (dots), Scalebar = 5µm. **K)** Percentage of cells with 0, 1, 2, 3, 4 or ≤ 5 PLA interaction dots (n = 3, biological repeats equal to an average of 203/211 and 376 (young control/OE, old control) cells per replicate). **L)** PLA signal (Ube2g1-Shp2) per cell normalised to young control (n = 3, biological repeats equal to an average of 203/211 and 376 (young control/OE, old control) cells per replicate). Data show individual biological replicates with each replicate as mean ± SD. Data were assessed by a One sample t test against a value of 0 for young control (C, D, F-G, L) or a non-parametric Mann-Whitney test (H, I). *$p < 0.05$, **$p < 0.01$, ***$p < 0.001$, ****$p < 0.0001$.

Figure 5: Elevated levels of Ube2g1 results in attenuated T-cell development in the thymus and increased exhaustion in released peripheral T-cells

A) Schematic of the experimental set-up of the competitive transplantation experiment, using sorted HSCs from young (12-16 weeks, WT) and aged (>80 weeks, AcRFP$^+$) donor mice (CD45.2$^+$). HSCs were genetically engineered and transplanted alongside 5 x10^4 CD45.1$^+$ BM cells into lethally irradiated recipient mice (CD45.1$^+$). **B)** Representative flow cytometry plots showing thymocytes gated for young and aged CD4/CD8 double negative (DN) and positive (DP) cells. Single positive CD4 and CD8 cells were gated for CD3. DN cells (yellow box) were gated for CD3-negative and then for CD44/CD25 to identify DN subpopulations DN1-4 (DN1; CD44$^+$CD25$^-$, DN2; CD44$^+$CD25$^+$, DN3; CD44$^-$CD25$^+$, DN4; CD44$^-$CD25$^-$). Indicative DN1-4 gating for young control and OE derived thymocytes are depicted. **C)** Percentage of donor-derived (GFP$^+$) DN and DP cells in thymus 24 weeks post-

transplantation (n = 11-12). **D)** Percentage of donor-derived (GFP^+) DN1-4 cells in the thymus 24 weeks post-transplantation (n = 11-12). **E)** Percentage of donor-derived (GFP^+) single positive peripheral ($CD3^+$) CD4 and CD8 cells in the thymus 24 weeks post-transplantation (n = 11-12). **F)** Representative flow cytometry plots showing splenocytes gated for young and aged CD4/8-positive T-cell exhaustion markers CD366 (Tim-3) and CD279 (PD-1). Indicative Tim-3/PD-1 gating for young control and OE derived splenocytes are depicted. **G)** Percentage of donor-derived (GFP^+) Tim-3 and/or PD-1 exhaustion markers on $CD8^+$ T-cells in the spleen 24 weeks post-transplantation (n = 11-12). Data show individual biological replicates from two independent experiment repeats as mean ± SD. Data were assessed by One-Way ANOVA or Kruskal-Wallis test depending on normality (C-E, G). *p < 0.05, **p < 0.01, ***p < 0.001, ****p < 0.0001.

Figure 1

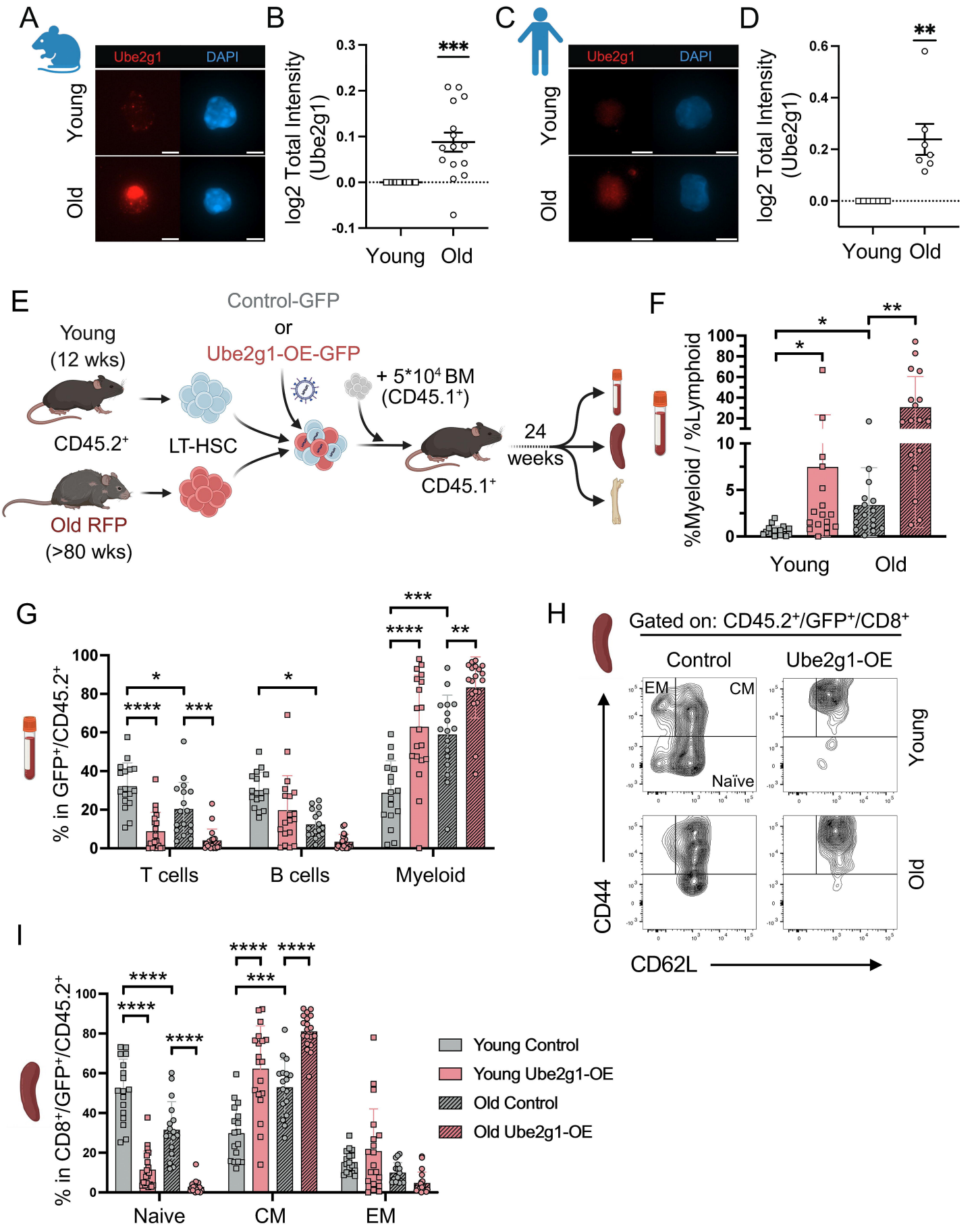
A
Ube2g1
DAPI
Young
Old
B
log2 Total Intensity (Ube2g1)
***
Young
Old
C
Ube2g1
DAPI
Young
Old
D
log2 Total Intensity (Ube2g1)
**
Young
Old
E
Young (12 wks)
CD45.2+
Old RFP (>80 wks)
LT-HSC
Control-GFP or Ube2g1-OE-GFP
+ 5*10^4 BM (CD45.1+)
CD45.1+
24 weeks
F
%Myeloid / %Lymphoid
Young
Old
G
% in GFP+/CD45.2+
T cells
B cells
Myeloid
H
Gated on: CD45.2+/GFP+/CD8+
Control
Ube2g1-OE
EM
CM
Naïve
Young
Old
CD44
CD62L
I
% in CD8+/GFP+/CD45.2+
Naive
CM
EM
Young Control
Young Ube2g1-OE
Old Control
Old Ube2g1-OE

Figure 2

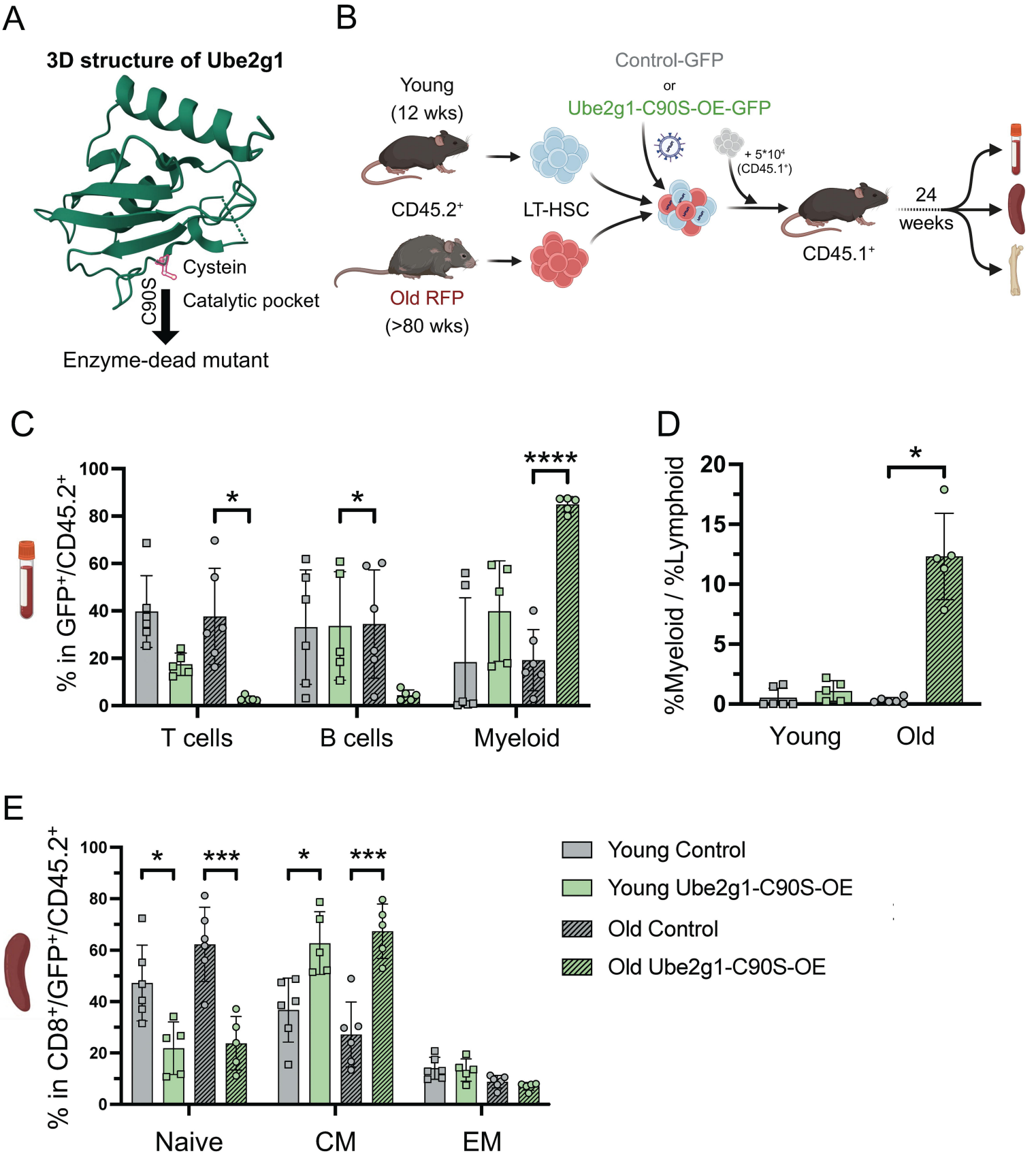
A
3D structure of Ube2g1
Cystein
C90S
Catalytic pocket
Enzyme-dead mutant
B
Young
(12 wks)
CD45.2+
Old RFP
(>80 wks)
LT-HSC
Control-GFP
or
Ube2g1-C90S-OE-GFP
+ 5*10^4
(CD45.1+)
CD45.1+
24
weeks
C
% in GFP+/CD45.2+
T cells
B cells
Myeloid
D
%Myeloid / %Lymphoid
Young
Old
E
% in CD8+/GFP+/CD45.2+
Naive
CM
EM
Young Control
Young Ube2g1-C90S-OE
Old Control
Old Ube2g1-C90S-OE

Figure 3

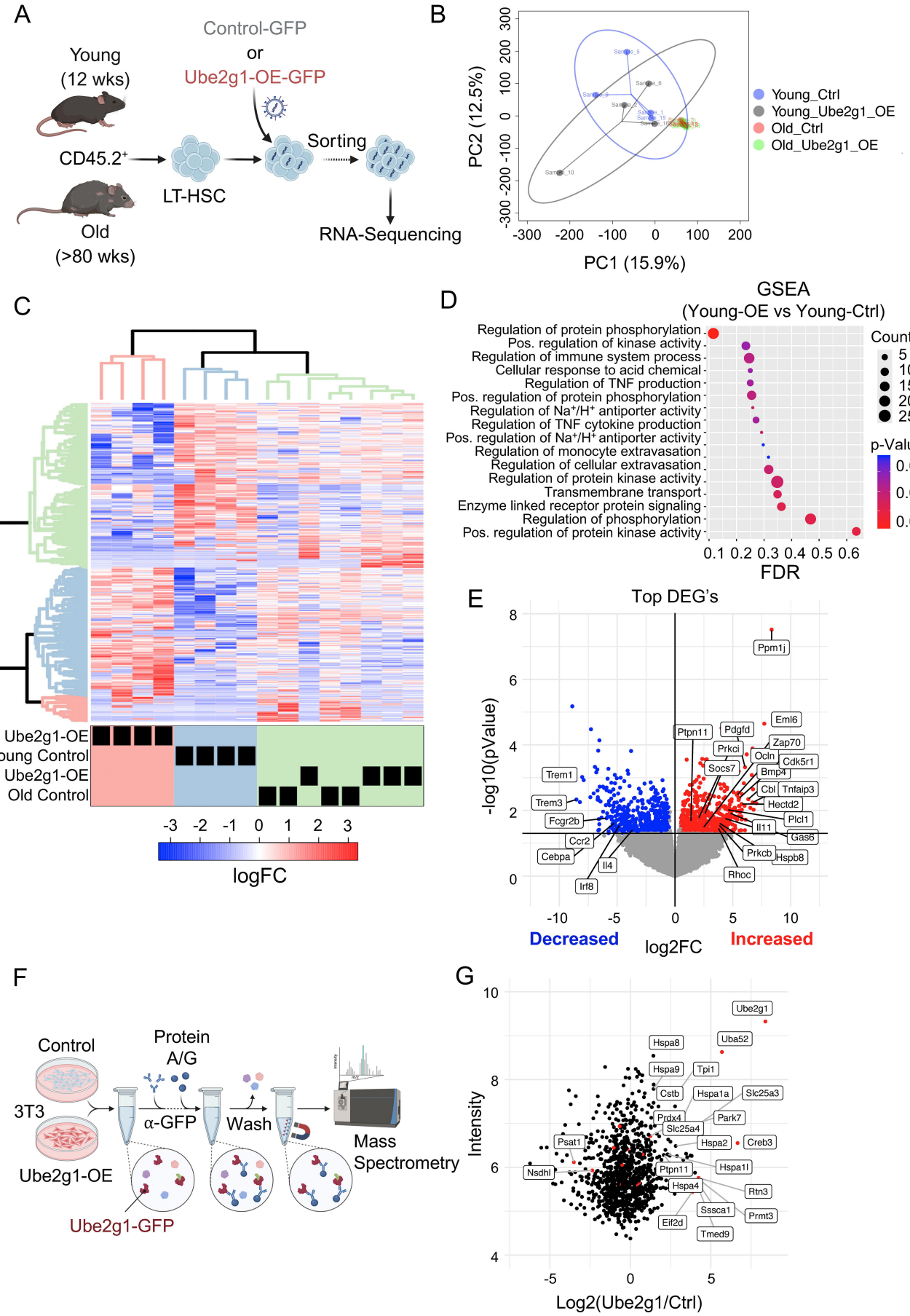
A
Young
(12 wks)
Control-GFP
or
Ube2g1-OE-GFP
CD45.2+
LT-HSC
Sorting
Old
(>80 wks)
RNA-Sequencing
B
PC2 (12.5%)
PC1 (15.9%)
Young_Ctrl
Young_Ube2g1_OE
Old_Ctrl
Old_Ube2g1_OE
C
Young Ube2g1-OE
Young Control
Old Ube2g1-OE
Old Control
logFC
D
GSEA
(Young-OE vs Young-Ctrl)
Regulation of protein phosphorylation
Pos. regulation of kinase activity
Regulation of immune system process
Cellular response to acid chemical
Regulation of TNF production
Pos. regulation of protein phosphorylation
Regulation of Na+/H+ antiporter activity
Regulation of TNF cytokine production
Pos. regulation of Na+/H+ antiporter activity
Regulation of monocyte extravasation
Regulation of cellular extravasation
Regulation of protein kinase activity
Transmembrane transport
Enzyme linked receptor protein signaling
Regulation of phosphorylation
Pos. regulation of protein kinase activity
FDR
Count
p-Value
E
Top DEG's
-log10(pValue)
log2FC
Decreased
Increased
Ppm1j
Eml6
Ptpn11
Pdgfd
Zap70
Prkci
Ocln
Cdk5r1
Socs7
Bmp4
Trem1
Cbl
Tnfaip3
Trem3
Hectd2
Fcgr2b
Plcl1
Il11
Gas6
Ccr2
Cebpa
Il4
Prkcb
Hspb8
Irf8
Rhoc
F
Control
3T3
Ube2g1-OE
Protein
A/G
α-GFP
Wash
Mass
Spectrometry
Ube2g1-GFP
G
Intensity
Log2(Ube2g1/Ctrl)
Ube2g1
Uba52
Hspa8
Hspa9
Tpi1
Cstb
Hspa1a
Slc25a3
Prdx4
Park7
Slc25a4
Psat1
Hspa2
Creb3
Nsdhl
Ptpn11
Hspa1l
Hspa4
Rtn3
Sssca1
Prmt3
Eif2d
Tmed9

Figure 4

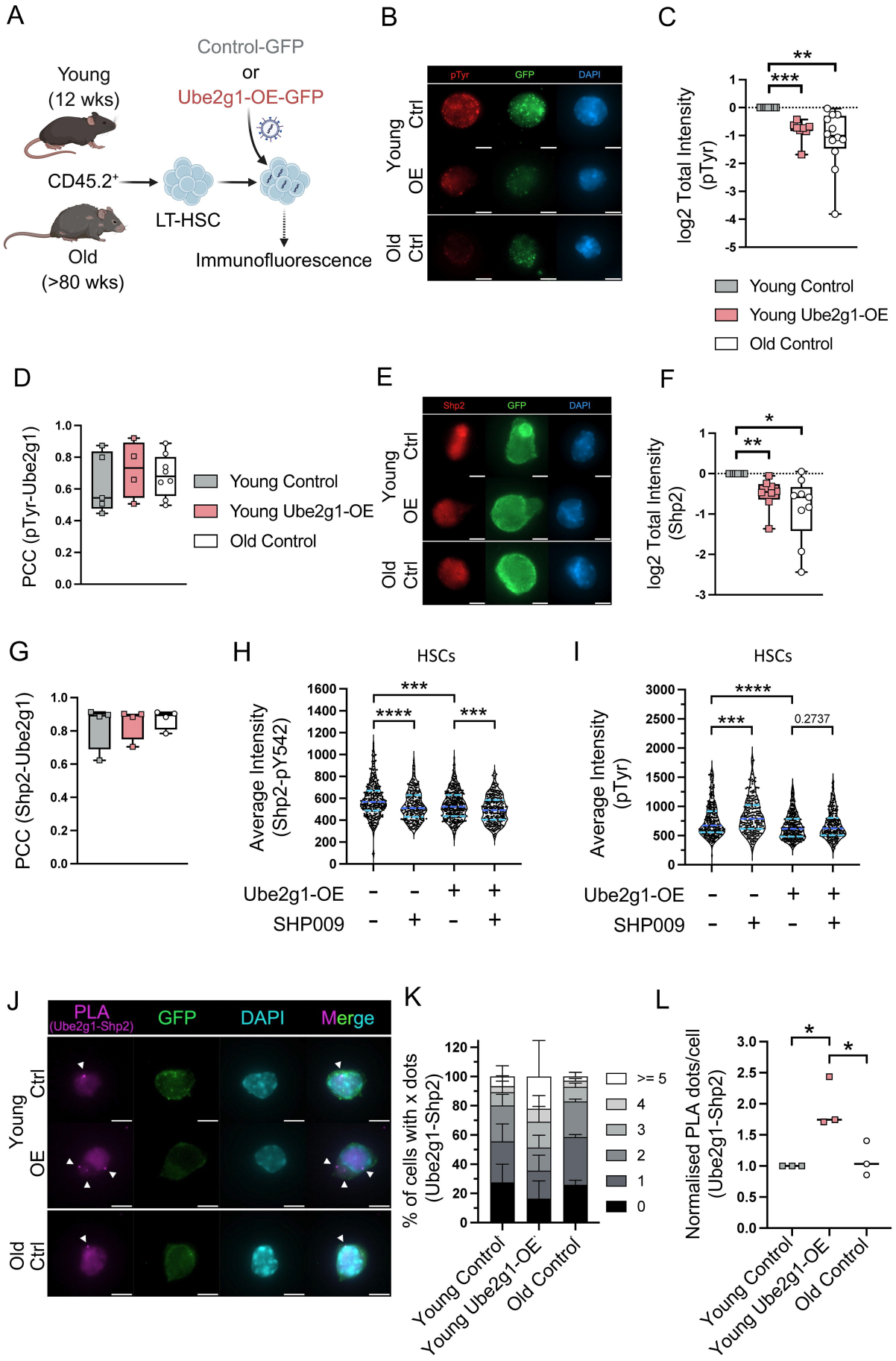
A
Young
(12 wks)
Control-GFP
or
Ube2g1-OE-GFP
CD45.2+
LT-HSC
Old
(>80 wks)
Immunofluorescence
B
pTyr
GFP
DAPI
Young Ctrl
OE
Old Ctrl
C
log2 Total Intensity (pTyr)
Young Control
Young Ube2g1-OE
Old Control
D
PCC (pTyr-Ube2g1)
E
Shp2
F
log2 Total Intensity (Shp2)
G
PCC (Shp2-Ube2g1)
H
HSCs
Average Intensity (Shp2-pY542)
Ube2g1-OE
SHP009
I
HSCs
Average Intensity (pTyr)
0.2737
J
PLA (Ube2g1-Shp2)
GFP
DAPI
Merge
K
% of cells with x dots (Ube2g1-Shp2)
>= 5
L
Normalised PLA dots/cell (Ube2g1-Shp2)

Figure 5

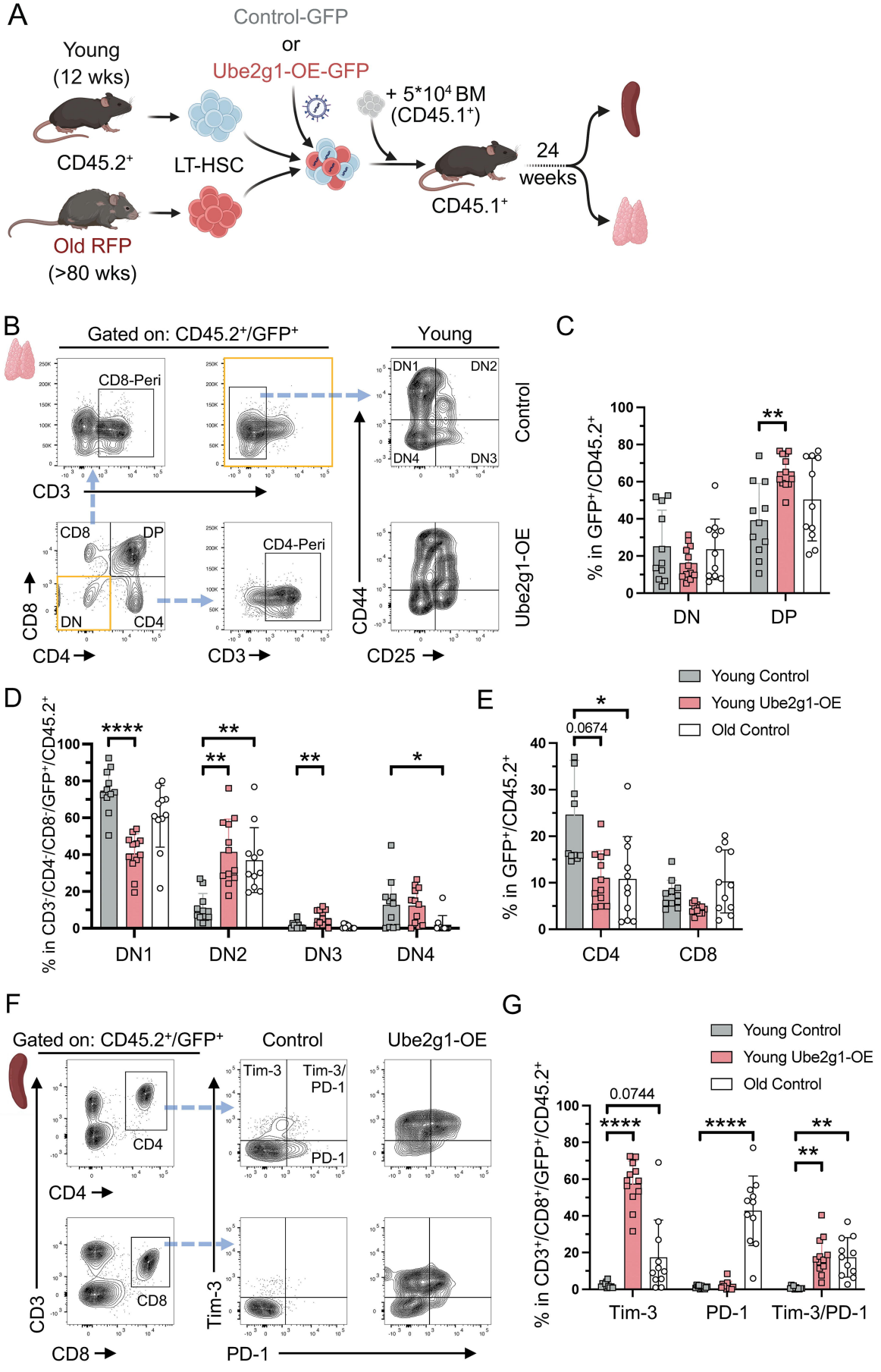
A
Young
(12 wks)
CD45.2+
Old RFP
(>80 wks)
LT-HSC
Control-GFP
or
Ube2g1-OE-GFP
+ 5*10^4 BM
(CD45.1+)
CD45.1+
24
weeks
B
Gated on: CD45.2+/GFP+
Young
CD8-Peri
CD3
CD8
DP
DN
CD4
CD4-Peri
DN1
DN2
DN4
DN3
Control
Ube2g1-OE
CD44
CD25
C
% in GFP+/CD45.2+
DN
DP
D
% in CD3-/CD4-/CD8-/GFP+/CD45.2+
DN1
DN2
DN3
DN4
E
Young Control
Young Ube2g1-OE
Old Control
0.0674
% in GFP+/CD45.2+
CD4
CD8
F
Gated on: CD45.2+/GFP+
Control
Ube2g1-OE
CD4
CD8
Tim-3
Tim-3/
PD-1
PD-1
G
Young Control
Young Ube2g1-OE
Old Control
0.0744
% in CD3+/CD8+/GFP+/CD45.2+
Tim-3
PD-1
Tim-3/PD-1

Supplementary Information

Elevated levels of Ube2g1 in hematopoietic stem cells lead to segmental aging of the hematopoietic system

Julian Niemann[1], Tanja Schuster[1], Vadim Sakk[1], Karin Soller[1], Andreas Brown[1], Sebastian Wiese[2], Karina Eiwen[1], Markus Hoenicka[3], Andreas Liebold[3], Moritz Oltmanns[4], Heiko Reichel[4], Medhanie A. Mulaw[5], Hartmut Geiger[1]

[1]Institute of Molecular Medicine, Ulm University, Germany,
[2]Core Unit Mass Spectrometry and Proteomics, Ulm University, Germany,
[3]Department of Cardiothoracic and Vascular Surgery, University Hospital, 89081 Ulm, Germany,
[4]Department of Orthopaedic Surgery, University Hospital, 89081, Ulm, Germany.
[5]Single-Cell Sequencing Unit, Ulm University, Germany

Supplementary Methods

RT-PCR

TaqMan technology (Thermo Fisher Scientific) was used to determine the level of expression of genes. Quantification was done using the $\Delta\Delta C_T$ method[48].

Immunoprecipitation and Western Blotting

Cell lysates were prepared using NP-40 lysis buffer[49] (50 mM Tris-HCl pH 8.0, 150 mM NaCl, 1% IGEPAL CA-630). For IP, antibodies were crosslinked to Dynabeads A/G (Thermo Fisher Scientific) using BS3 and incubated with lysates overnight at 4°C. For western blotting, lysates were separated by SDS-PAGE, transferred to PVDF membranes, and probed with antibodies (**Supplementary Table 1**).

T-cell activation assay

The CD8 T-cell Isolation kit (Miltenyi) and the Dynabeads Mouse T-cell CD3/CD28 Activator Kit (Thermo Fisher) were used to isolate and activate $CD8^+$ T-cells from single cell splenocytes of young and aged C57/BL6J wildtype mice. T-cells were activated and transduced overnight in TexMACS (MOI: 30; TexMACS with 50 U/mL rhIL-2) before culture for up to 48 hours until analysis.

Supplementary Figure Legends

Supplementary Figure 1: Expression of degradation specific ubiquitin is increased in aged murine HSC and aged human HSPCs

A) Schematic of the mutagenesis screen performed using a SFß91- based retroviral insertion to identify genes relevant for clonal selection of Lin-negative bone marrow (BM) cells. Upstream of the insertion site (blue arrow) Ube2g1 was identified to show increased expression in the clonally selected BM cells. **B)** Representative IF-pictures from young (12-16 weeks, WT) and aged (>80 weeks, AcRFP$^+$) murine hematopoietic stem cells (HSCs) stained for Ubiquitin (yellow) and DAPI (blue), Scalebar = 5µm. **C)** Relative (log2 transformed) intensity of Ubiquitin in young and old murine HSCs (n = 7-10, biological repeats equal to an average of 79/143 (young/old) cells per replicate). **D)** Representative IF-pictures of young and old murine HSCs stained for K48-Ubiquitin (green) and DAPI, Scalebar = 5µm. **E)** Relative (log2 transformed) intensity of K48-Ubiquitin in young and old murine HSCs (n = 7-10, biological repeats equal to an average of 79/143 (young/old) cells per replicate). **F)** Representative IF-pictures of human CD34$^+$ HSPCs from young (25-33 years donors; Mean = 30y) and old (55-80 years; Mean = 68y) donors stained for Ubiquitin (yellow) and DAPI (blue), Scalebar = 5µm. **G)** Relative (log2 transformed) intensity of Ubiquitin in young and old human CD34$^+$ HSPCs (n = 6, three young and six old biological repeats equal to an average of 199/178 (young/old) cells per replicate). **H)** Representative pictures of human HSPCs from young and old donors stained for K48-Ubiquitin (green) and DAPI, Scalebar = 5µm. **I)** Relative (log2 transformed) intensity of K48-Ubiquitin in young and old human CD34$^+$ HSPCs (n = 5, four young old biological repeats equal to an average of 191/166 (young/old) cells per replicate). Data show log2 transformed total intensity of individual replicates with each replicate as mean ± SEM. Data were assessed by a One sample t test against a value of 0 for young control (C, E, G, I). **p < 0.01.

Supplementary Figure 2: Elevated levels of Ube2g1 result in segmental premature aging of peripheral hematopoiesis

A) Relative (log2 transformed) gene expression of Ube2g1 two days post-transduction in HSPCs derived from young (12-16 weeks, WT) and aged (>80 weeks, AcRFP$^+$) mice (n = 5-8). **B)** Relative (normalised to young control) intensity of Ube2g1 in young control and Ube2g1-OE transduced murine HSCs (n = 3, biological repeats equal to an average of 308/274 (young control/OE) cells per replicate). **C)** Level of GFP in NIH/3T3 cells stably transduced with Control or Ube2g1-OE fusion protein, determined by Western Blot. The number below the panel indicates the normalisation factor based on total protein quantification. An asterisk (*) indicates Ube2g1-OE-GFP fusion protein (~50 kDa) and a

hashtag (#) GFP (~30 kDa). **D)** Level of Ube2g1 protein in NIH/3T3 cells stably transduced with Control or Ube2g1-OE, determined by Western Blot. The factor below the panel indicates the normalisation factor based on total protein quantification. Left panel shows a data from a short and right panel a longer exposure of the membrane. An asterisk (*) indicates Ube2g1-OE-GFP fusion protein (~50 kDa) and a hashtag (#) endogenous Ube2g1 (~20 kDa). **E)** Percentage of donor-derived (GFP^+) T-cells ($CD3e^+$), B-cells ($CD19^+$) and myeloid cells ($Gr\text{-}1^+/CD11^+$) in the spleen 24 weeks post-transplantation (n = 17-19). **F)** Ratio of the percentage of donor-derived (GFP^+) myeloid over lymphoid cells in the spleen 24 weeks post-transplantation (n = 16-19). **G)** Percentage of donor-derived (GFP^+) T-cells, B-cells and myeloid cells in the BM 24 weeks post-transplantation (n = 17-19). **H)** Ratio of the percentage of donor-derived (GFP^+) myeloid over lymphoid cells in the BM 24 weeks post-transplantation (n = 16-17). **I)** Percentage of donor-derived (GFP^+) HSCs ($CD34^{low}$, Lin^-, $Sca1^+$, $c\text{-}Kit^+$) in the BM 24 weeks post-transplantation (n = 17-19). **J)** Percentage of donor-derived (GFP^+) myeloid progenitors MEP (Lin^-, $c\text{-}Kit^+$, $CD34^{low}$, $CD16/32^-$), CMP (Lin^-, $c\text{-}Kit^+$, $CD34^+$, $CD16/32^-$) and GMP (Lin^-, $c\text{-}Kit^+$, $CD16/32^+$) in the BM 24 weeks post-transplantation (n = 17-19). **K)** Percentage of donor-derived (GFP^+) naïve and memory $CD4^+$ T-cells in the spleen 24 weeks post-transplantation (n = 11-12). Data show individual biological replicates from four independent experiment repeats as mean ± SD. Data were assessed by One-Way ANOVA or Kruskal-Wallis test depending on normality (A, B, E-K). *p < 0.05, **p < 0.01, ***p < 0.001, ****p < 0.0001.

Supplementary Figure 3: Reduced levels of Ube2g1 result in segmental rejuvenation of aged HSCs

A) Relative (log2 transformed) gene expression of Ube2g1 of a mixed HSC population two days post- transduction in cells derived from young (12-16 weeks, WT) and aged (>80 weeks, $AcRFP^+$) mice (n = 4-7). **B)** Level of Ube2g1 in NIH/3T3 cells stably transduced with Scrambled (Control) or Ube2g1-KD, determined by Western Blot. The factor below the panel indicates the normalisation factor based on total protein quantification. Arrow indicates endogenous Ube2g1 (~20 kDa). **C)** Relative (normalised to old control) intensity of Ube2g1 in old control and Ube2g1-KD transduced murine HSCs (n = 4, biological repeats equal to an average of 770/582 (old control/KD) cells per replicate). **D)** Schematic of the experimental set-up of the competitive transplantation experiment, using sorted HSCs from young (12-16 weeks, WT) and aged (>80 weeks, $AcRFP^+$) donor mice ($CD45.2^+$). HSCs were genetically engineered and transplanted alongside 5 $x10^4$ $CD45.1^+$ BM cells into lethally irradiated recipient mice ($CD45.1^+$). **E)** Ratio of the percentage of donor-derived (GFP^+) myeloid over lymphoid cells in PB 24 weeks post-transplantation (n = 7-9). **F)** Percentage of donor-derived (GFP^+) T-cells ($CD3e^+$), B-cells ($CD19^+$) and myeloid cells ($Gr\text{-}1^+/CD11^+$) in PB 24

weeks post-transplantation (n = 9-11). **G)** Percentage of donor-derived (GFP^+) naïve, CM and EM $CD8^+$ T-cells in the spleen 24 weeks post-transplantation (n = 12-13). **H)** Ratio of the percentage of donor-derived (GFP^+) myeloid over lymphoid cells in the spleen 24 weeks post- transplantation (n = 12-13). **I)** Percentage of donor-derived (GFP^+) T-cells, B-cells and myeloid cells in the BM 24 weeks post-transplantation (n = 11-13). **J)** Percentage of donor-derived (GFP^+) HSCs ($CD34^{low}$, Lin^-, $Sca1^+$, $c\text{-}Kit^+$) in the BM 24 weeks post-transplantation (n = 12-13). Data show individual biological replicates from two independent experiment repeats as mean ± SD. Data were assessed by One-Way ANOVA or Kruskal-Wallis test depending on normality (A, C, E-J). *p < 0.05, **p < 0.01, ***p < 0.001, ****p < 0.0001.

Supplementary Figure 4: Characterisation of Ube2g1-C90S-OE HSCs in spleen and bone marrow of transplanted mice

A) Schematic of sequencing of plasmids after site directed mutagenesis (SDM) for Ube2g1-C90S in genetically engineered NIH/3T3s cells. **B)** Level of GFP in NIH/3T3 cells stably transduced with Control, Ube2g1-OE and $Ube2g1^{C90S}$-OE, determined by Western Blot. The factor below the panel indicates the normalisation factor based on total protein quantification. Arrows indicate expressed Ube2g1-OE-GFP fusion protein (~50 kDa) and GFP (~30 kDa). **C)** Level of Ube2g1 in NIH/3T3 cells stably transduced with Control, Ube2g1-OE and $Ube2g1^{C90S}$-OE, determined by Western Blot. The factor below the panel indicates the normalisation factor based on total protein quantification. Left panel shows a low and right panel a high luminescence exposure. Arrows indicate expressed Ube2g1-OE-GFP fusion protein (~50 kDa) and endogenous Ube2g1 (~20 kDa). **D)** Relative (normalised to young control) intensity of Ube2g1 in young control, Ube2g1-OE and Ube2g1-C90S-OE transduced murine HSCs (n = 3, biological repeats equal to an average of 308/274/237 (young control/OE/C90S) cells per replicate). **E)** Percentage of donor-derived (GFP^+) T-cells ($CD3e^+$), B-cells ($CD19^+$) and myeloid cells ($Gr\text{-}1^+/CD11^+$) in the spleen 24 weeks post-transplantation (n = 5-6). **F)** Ratio of the percentage of donor-derived (GFP^+) myeloid over lymphoid cells in the spleen 24 weeks post-transplantation (n = 5-6). **G)** Percentage of donor-derived (GFP^+) T-cells, B-cells and myeloid cells in the BM 24 weeks post-transplantation (n = 5-6). **H)** Percentage of donor-derived (GFP^+) HSCs in the BM 24 weeks post-transplantation (n = 5-6). **I)** Percentage of donor-derived (GFP^+) myeloid progenitors MEP (Lin^-, $c\text{-}Kit^+$, $CD34^{low}$, $CD16/32^-$), CMP (Lin^-, $c\text{-}Kit^+$, $CD34^+$, $CD16/32^-$) and GMP (Lin^-, $c\text{-}Kit^+$, $CD16/32^+$) in the BM 24 weeks post-transplantation (n = 5-6). Data show individual biological replicates as mean ± SD. Data were assessed by One-Way ANOVA or Kruskal-Wallis test depending on normality (D-I). *p < 0.05, **p < 0.01, ***p < 0.001, ****p < 0.0001.

Supplementary Figure 5: PLA specificity controls and validation of Uba52 and Creb3 as Ube2g1 interactor

A) Ube2g1 levels for immunoprecipitation (IP) processed samples of control and Ube2g1-OE NIH/3T3 cells, determined by Western Blot. IP was performed based on anti-IgG or -GFP antibody. Samples are grouped as input, IgG Control IP and anti-GFP IP. Highlighted are endogenous Ube2g1 as well as Ube2g1-GFP fusion protein. **B)** Uba52 levels for immunoprecipitation (IP) processed samples of control and Ube2g1-OE NIH/3T3 cells, determined by Western Blot. IP was performed based on anti-IgG or -GFP antibody. Samples are grouped as input, IgG Control IP and anti-GFP IP. Highlighted are endogenous Uba as well as a likely Ube2g1-Uba52 protein complex. **C)** Representative IF-pictures from young and old control and young Ube2g1-OE transduced murine HSCs stained for Hsf1 (orange), GFP (green) and DAPI (blue), Scalebar = 5µm. **D)** Relative (log2 transformed) intensity of Hsf1 in young and old control and young Ube2g1-OE transduced murine HSCs (n = 5, biological repeats equal to an average of 116/130 and 171/150 (young control/OE, old control/OE) cells per replicate). **E)** Proximity Ligation assay (PLA) controls without primary antibody (No 1^{st}-Ab) as well as an IgG-Rb control instead of Ube2g1 in a PLA with Shp2 at the same concentration. All controls were performed in old control cells to acknowledge the potential influence of GFP counterstaining. For better comparability of values, three young control samples Ube2g1-Shp2 PLAs were added to the graph for better visualisation. **F)** Representative IF-pictures from old control, Ube2g1-OE and Ube2g1-C90S-OE transduced murine HSCs showing PLA signal (Ube2g1-Uba52) with counterstaining for GFP and DAPI, White arrows indicate PLA interactions (dots), Scalebar = 5µm. **G)** Percentage of cells with 0, 1, 2, 3, 4 or ≤ 5 dots (n = 3-5, biological repeats equal to an average of 907/947/492 (old control/OE/C90S) cells per replicate). **H)** PLA signal (Ube2g1-Uba52) per cell normalised to young control (n = 3-5, biological repeats equal to an average of 907/947/492 (old control/OE/C90S) cells per replicate). **I)** Representative IF-pictures from old control and Ube2g1-OE transduced murine HSCs showing PLA signal (Ube2g1-Creb3) with counterstaining for GFP and DAPI, White arrows indicate PLA interactions (dots), Scalebar = 5µm. **J)** Percentage of cells with 0, 1, 2, 3, 4 or ≤ 5 dots (n = 3, biological repeats equal to an average of 625/629 (old control/OE) cells per replicate). **K)** PLA signal (Ube2g1-Creb3) per cell normalised to young control (n = 3, biological repeats equal to an average of 625/629 (old control/OE) cells per replicate). Data show log2 transformed total intensity of individual biological replicates with each replicate as mean ± SD. Data were assessed by a One sample t test against a value of 0 for control samples or a non-parametric Mann-Whitney test (D, H, K). *$p < 0.05$, **$p < 0.01$.

Supplementary Figure 6: Multicolour staining confirmation and analysis of Shp2 and pTyr after knockdown and Ube2g1 mutation

A) Representative IF-pictures from young (12-16 weeks, WT) murine HSCs single colour stained either without primary antibody or with an antibody against GFP (green), Hsf1 (orange) or pTyr (red) followed by a mix of all corresponding secondary antibodies, Scalebar = 5µm. **B)** Total intensity of phosphorylated tyrosine (pTyr) in old control and Ube2g1-KD HSCs (n = 418/182 (old control/OE) from two biological replicates). **C)** Total intensity of Shp2 in old control and Ube2g1-KD HSCs (n = 218/337 (old control/OE) from two biological replicates). **D)** Total intensity of phosphorylated tyrosine (pTyr) in young control, Ube2g1-OE, Ube2g1-C90S-OE and old control HSCs (n = 82/93/79/208 cells (young control/OE/C90S/old control) from one biological replicate)). **E)** Total intensity of Shp2 in young control, Ube2g1-OE, Ube2g1-C90S-OE and old control HSCs (n = 104/71/60/119 cells (young control/OE/C90S/old control) from one biological replicate)). Data were assessed by non-parametric Mann-Whitney test (B-E). **p < 0.01, ****p < 0.0001.

Supplementary Figure 7: Young Ube2g1-OE T-cells show increased exhaustion and decreased TCR activation

A) Counts of donor-derived (GFP^+) total live DN and DP cells in the thymus 24 weeks post-transplantation (n = 11-12). **B)** Counts of donor-derived (GFP^+) total live DN1-4 cells in the thymus 24 weeks post-transplantation (n = 11-12) **C)** Percentage of donor-derived (GFP^+) Tim-3 and/or PD-1 exhaustion markers on $CD4^+$ T-cells in the spleen 24 weeks post-transplantation (n = 11-12). **D)** Schematic of the experimental setup for $CD8^+$ T-cell isolation, transduction and activation using MACS based isolation, CD3/CD28 activation beads and flow cytometry along with IF to analyse the cells. **E)** Percentage of $CD8^+$ T-cells in $CD3^+/GFP^+$ cells. $T_{0/24h/48}$ represent measurements after isolation, 24 hours and 48 hours post-transduction/activation (n = 4 biological replicates). **F)** Percentage of $CD69^+$ T-cells in $CD8^+/CD3^+/GFP^+$ cells. $T_{0/24h/48}$ represent measurements after isolation, 24 hours and 48 hours post-transduction/activation (n = 4 biological replicates). **G)** Total intensity of Ube2g1 in young control, Ube2g1-OE and old control HSCs 48 hours post-activation/transduction (n = 147/140/147 cells (young control/OE/old control) from one biological replicate)). **H)** Total intensity of phosphorylated tyrosine (pTyr) in young control, Ube2g1-OE and old control HSCs 48 hours post-activation/transduction (n = 145/148/148 cells (young control/OE/old control) from one biological replicate)). **I)** Total intensity of phosphorylated Shp2 (pY542) in young control, Ube2g1-OE and old control HSCs 48 hours post-activation/transduction (n = 146/148/148 cells (young control/OE/old control) from one biological replicate)). Data show individual biological replicates from two/four (A-C; E, F) independent experiment repeats as mean ± SD. Data were assessed by One-Way ANOVA or Kruskal-Wallis (A-C) and non-

parametric Mann-Whitney or unpaired student's t test (E-I) depending on normality. *p < 0.05, **p < 0.01, ***p < 0.001, ****p < 0.0001.

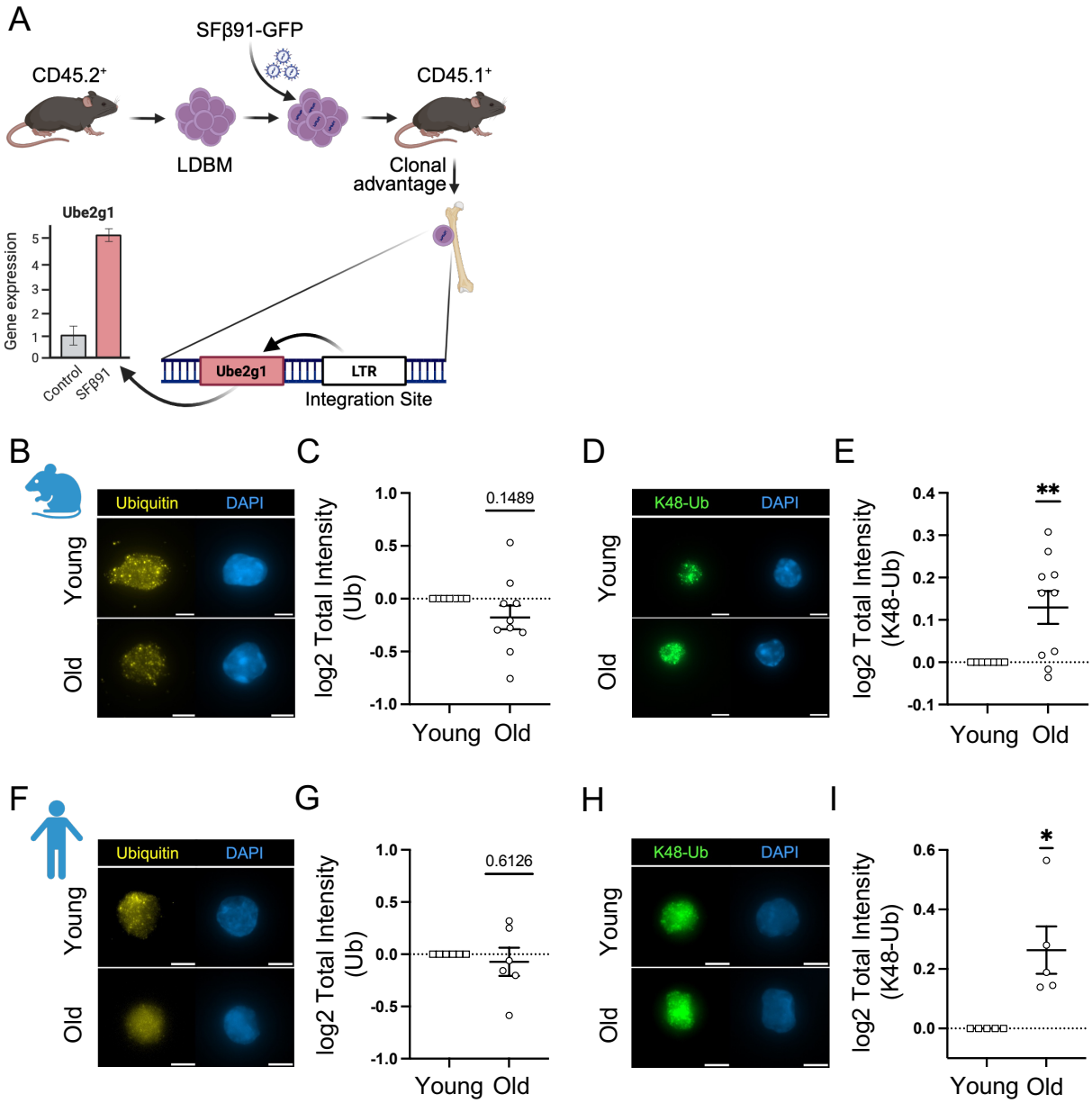

Supplementary Figure 1

Niemann *et al.*

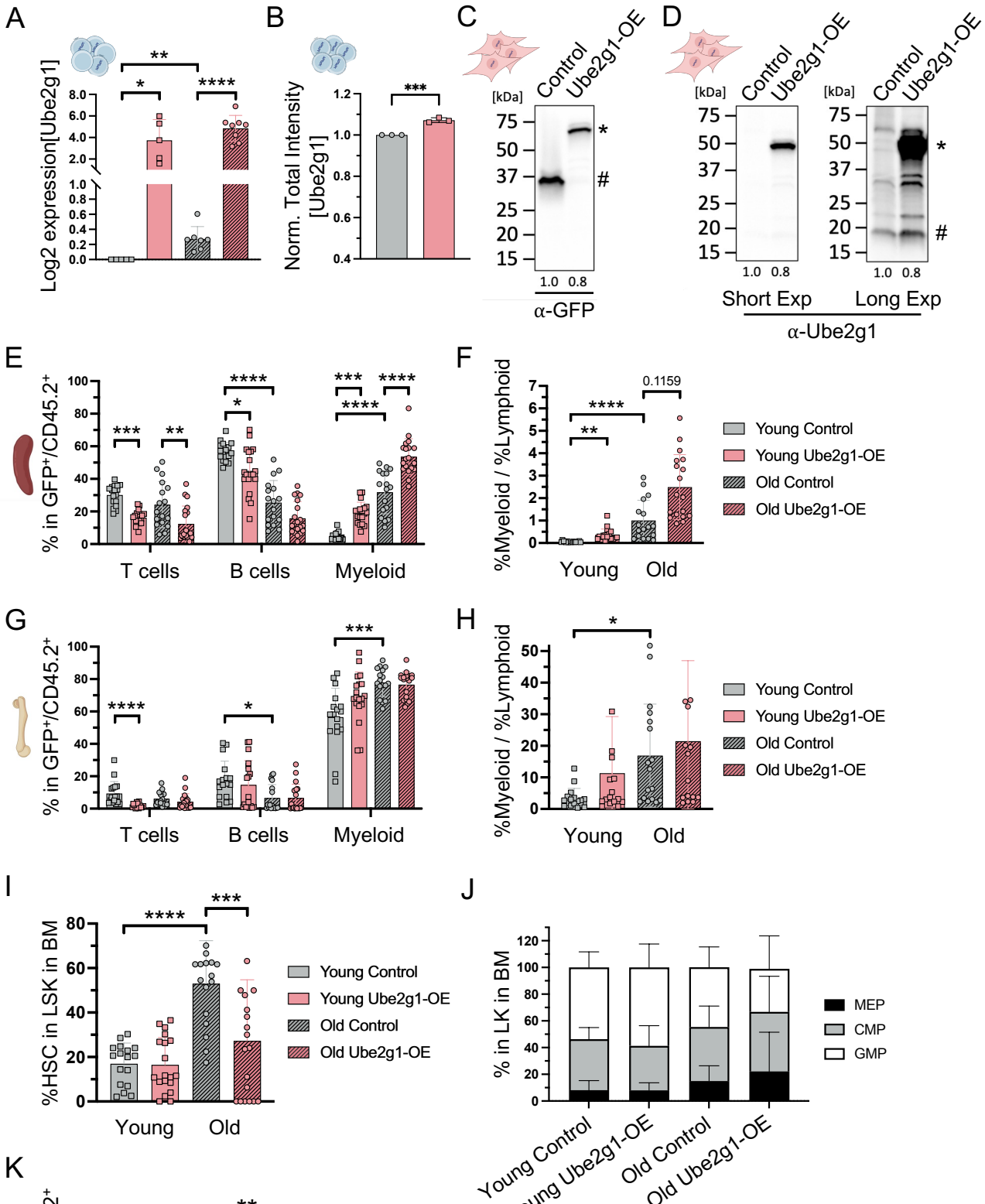

Supplementary Figure 2

Niemann *et al.*

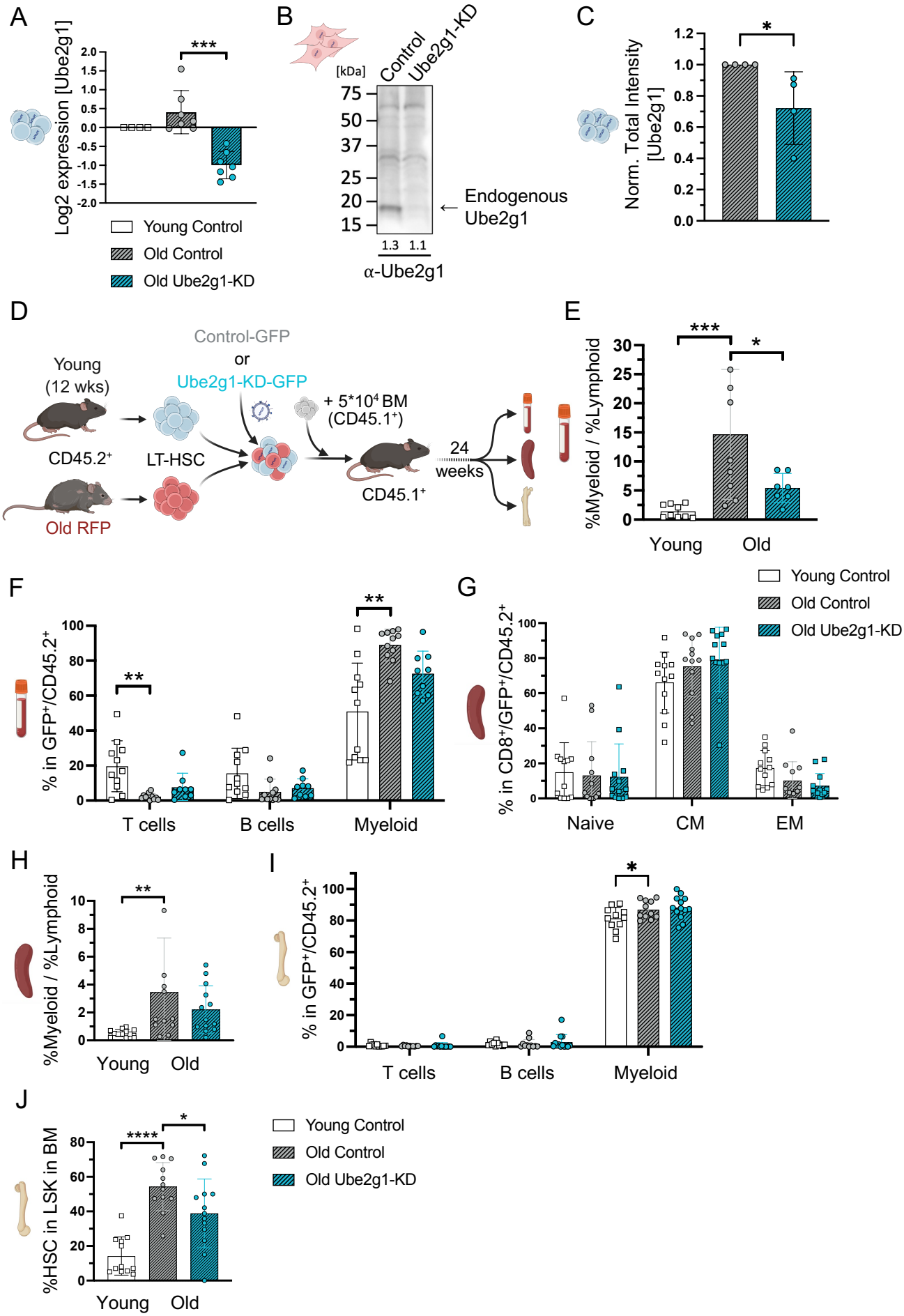

Supplementary Figure 3

Niemann *et al.*

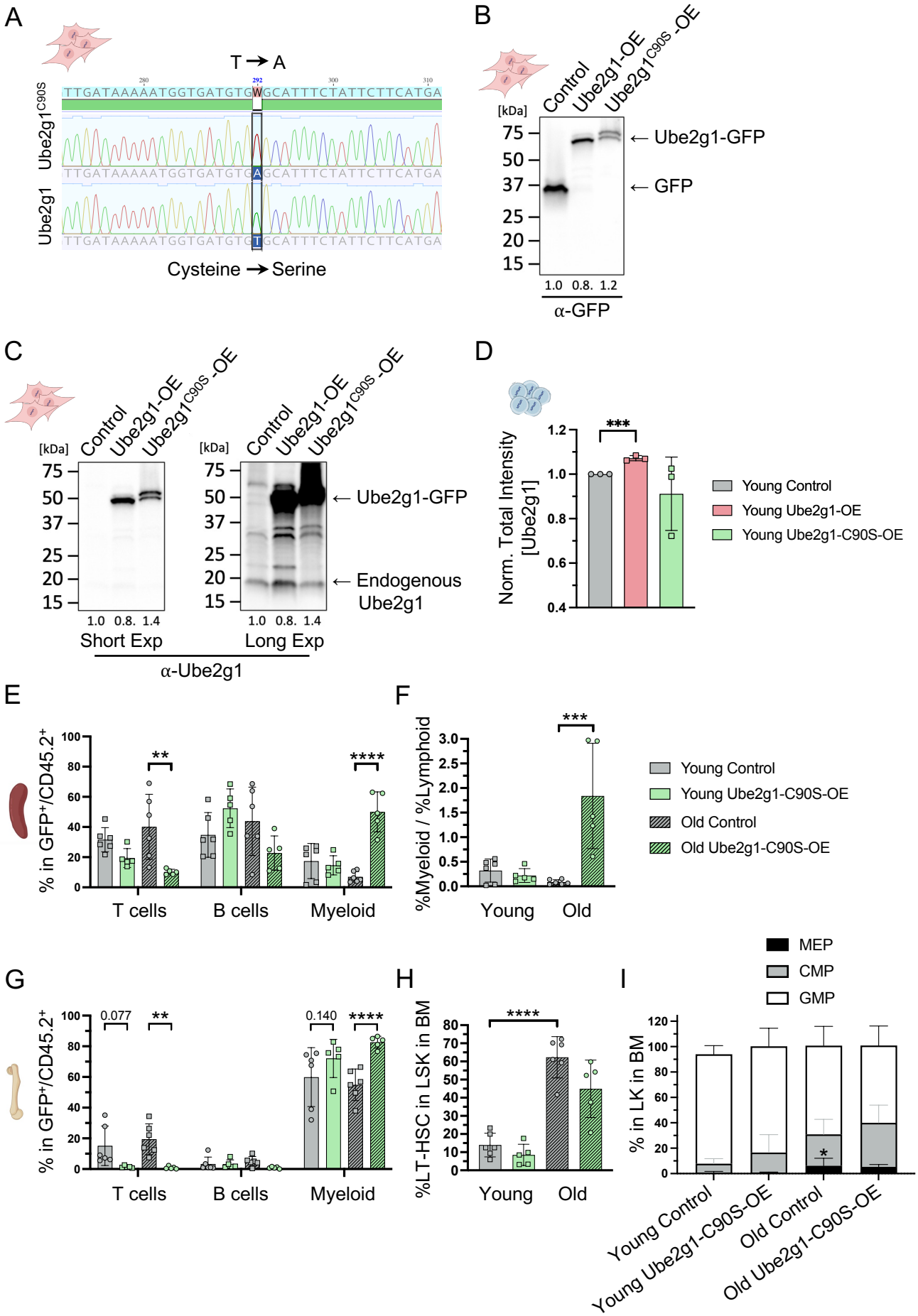

Supplementary Figure 4

Niemann *et al.*

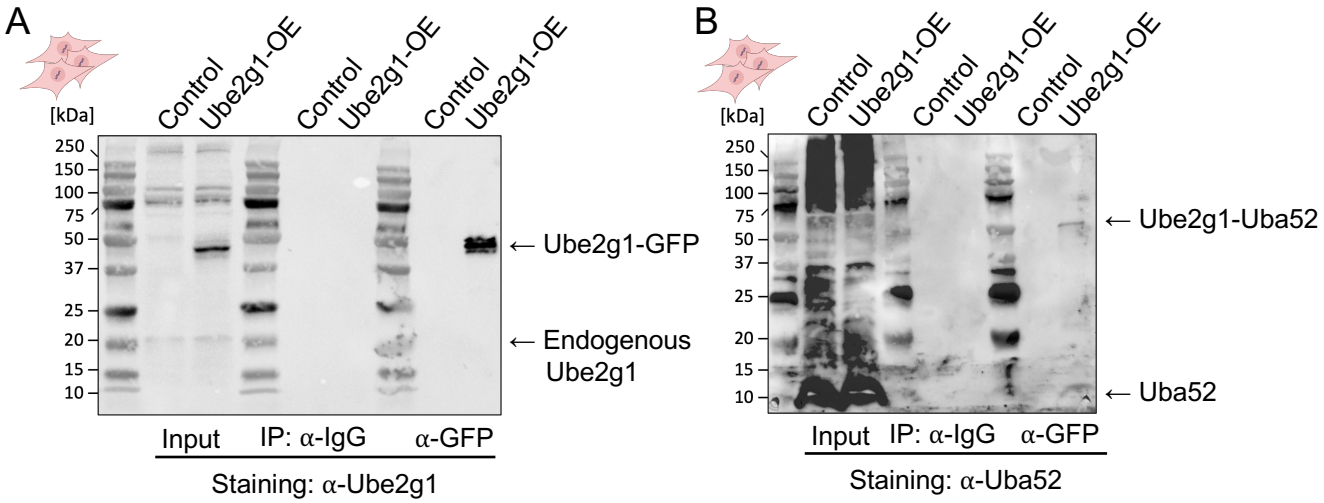

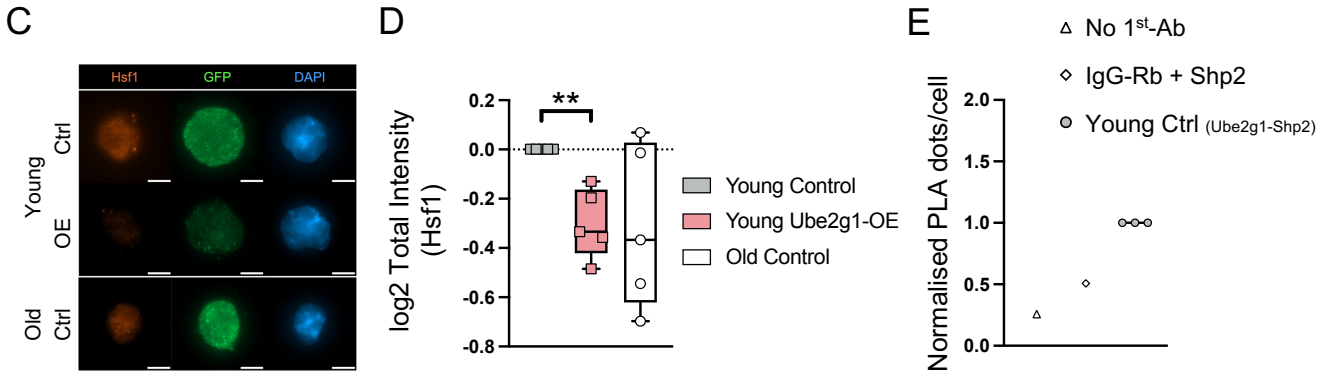

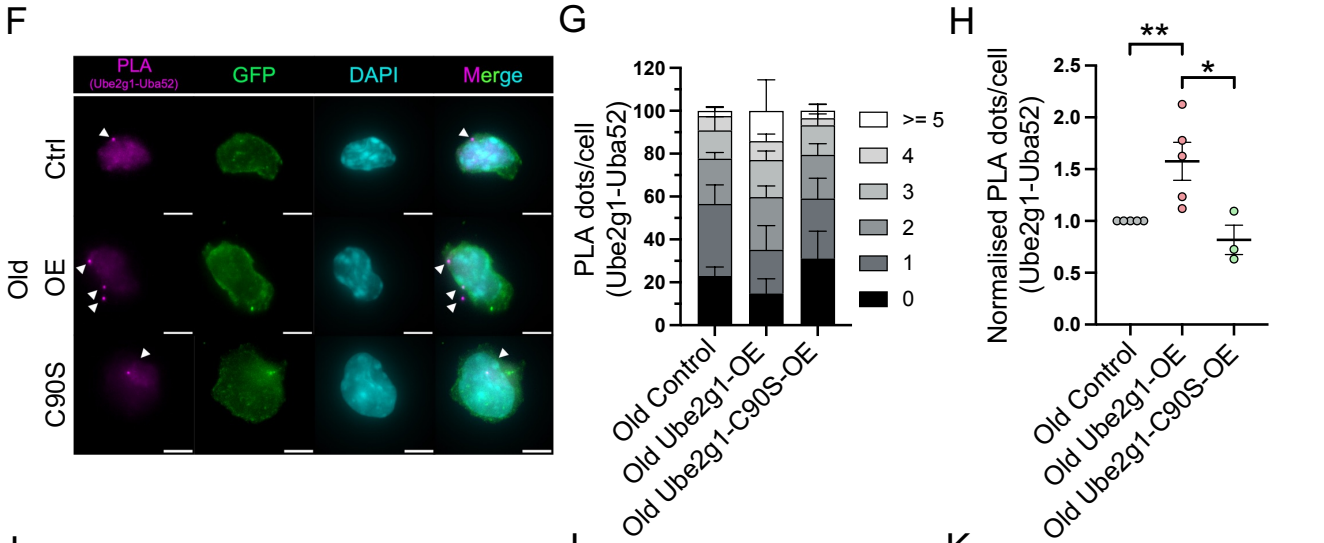

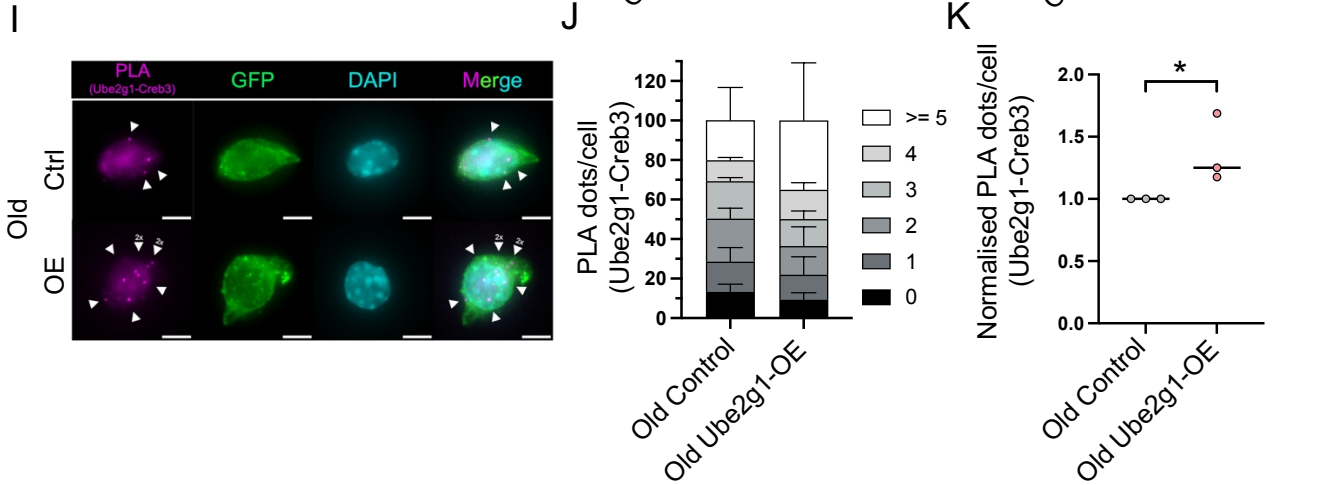

Supplementary Figure 5

Niemann *et al.*

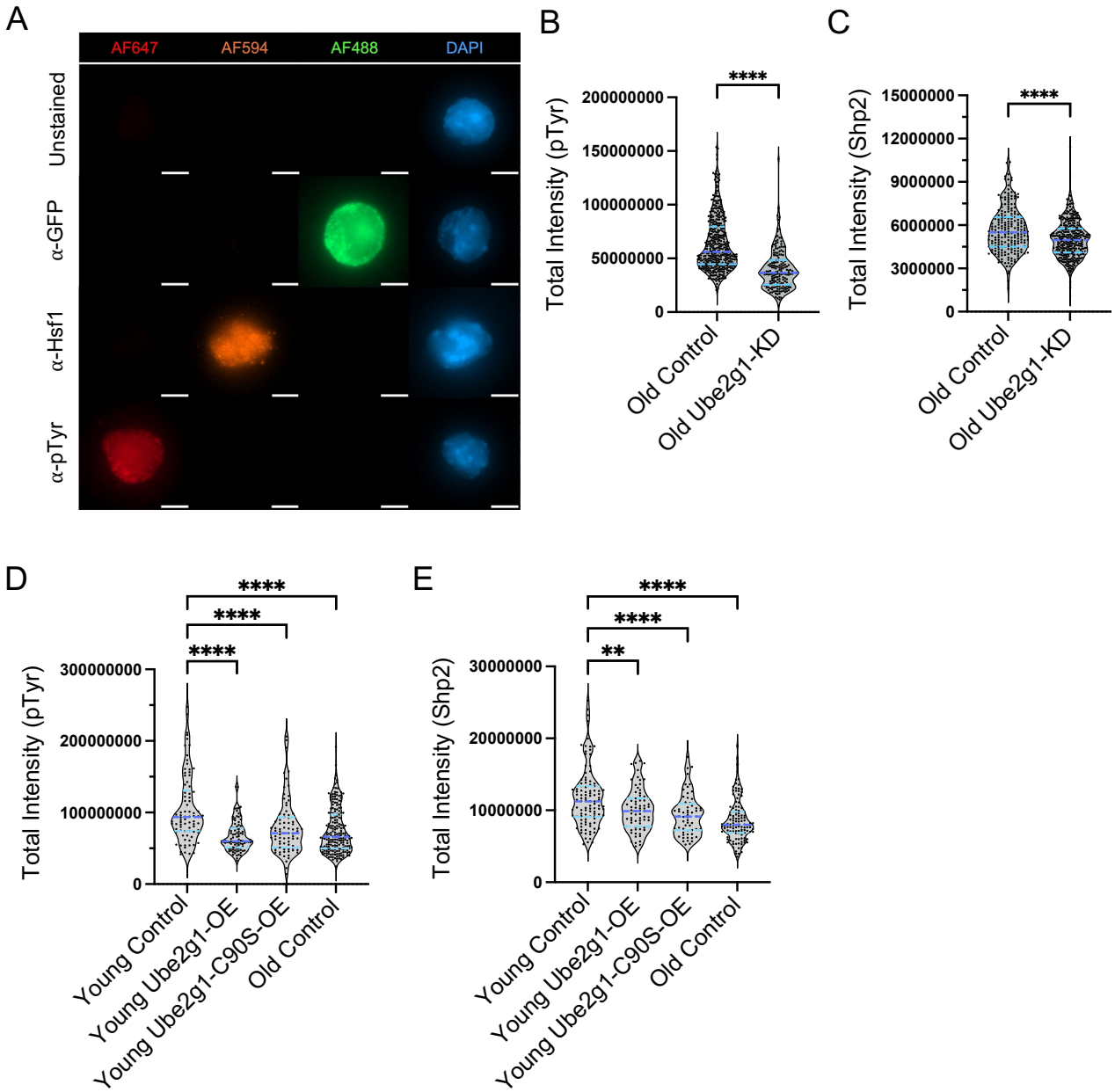

Supplementary Figure 6

Niemann *et al.*

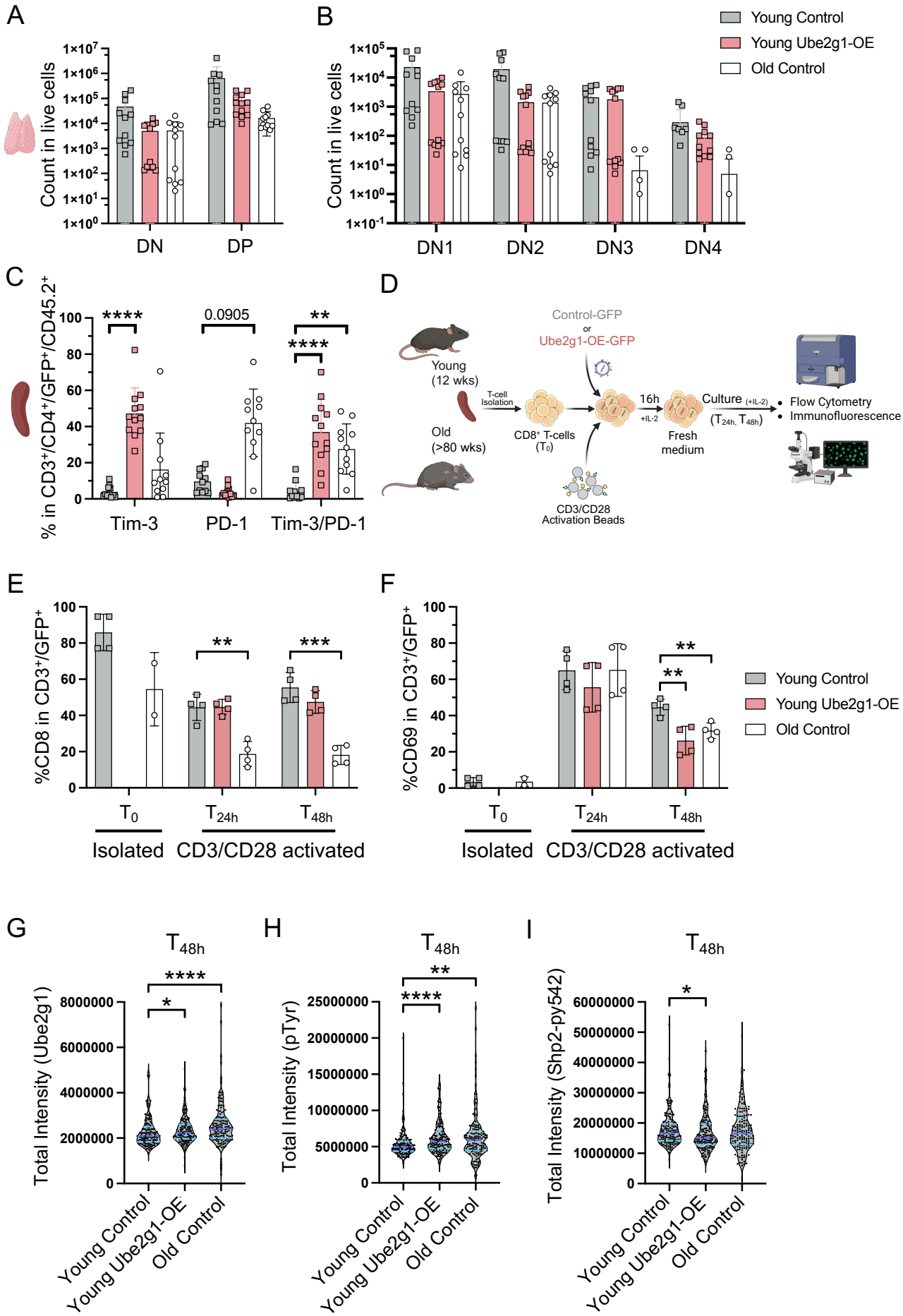

Supplementary Figure 7

Niemann *et al.*

Supplementary Table 1: Antibody Information

Flow Cytometry (FC)			
Antibody	**Conjugate**	**Vendor**	**Identifier**
CD8α	Pacific Blue	BD Biosciences	558106
CD16/32	APC-Cy7		560541
Streptavidin	eF450	eBioscience	48-4317-82
c-Kit	AlexaFluor 700		56-1172-82
Sca-1	PE-Cy7		25-5981-82
CD34	FITC		11-0341-85
CD34	APC		50-0341-82
Flt3	PE		12-1351-83
Ly6C/G (Gr-1)	eF450		48-5931-82
CD11b	AlexaFluor 700		56-0112-82
CD19	APC		17-0193-82
CD3ε	PE-Cy7		25-0031-82
	AlexaFluor 700	BioLegend	100216
CD44	PE-Cy7		103030
CD366 (Tim-3)	BrilliantViolet 605		119721
CD279 (PD-1)	PE/Dazzle 594		109115
CD4	APC	Thermo Fisher Scientific	17-0042-83
CD62L	PerCp-Cy5.5		45-0621-82
CD25	PerCp-Cy5.5		45-0251-80
CD45.2	APC-Vio770	Miltenyi Biotec	130-119-128

Immunofluorescence (IF)			
Antibody	**Species**	**Vendor**	**Identifier**
Ube2g1	Rabbit	Abcam	ab101371
K48-Ubiquitin	Rabbit		ab140601
GFP	Goat		ab6673
pTyr	Mouse		ab10321
Hsf1	Rabbit	Cell Signaling	4356S
Ubiquitin	Mouse	Thermo Fisher Scientific	PA-10023
Shp2	Mouse		MA5-36980
Shp2-pY542	Rabbit		44-554G
α-Mouse	AlexaFluor 647	Jackson ImmunoResearch	715-605-150
	AlexaFluor 594		715-585-150
	AlexaFluor 488		715-545-150
α-Rabbit	AlexaFluor 647		711-605-152
	AlexaFluor 594		711-585-152
	AlexaFluor 488		711-545-152
α-Goat	AlexaFluor 488		705-545-147

Western Blotting (WB)			
Antibody	**Species**	**Vendor**	**Identifier**
GFP	Goat	Abcam	ab6673
Ube2g1	Rabbit	Thermo Fisher Scientific	PA5-62212
Uba52	Rabbit	Abcam	ab109227
IgG	Goat	R&D Systems	AB-108-C
α-Rabbit	HRP	SouthernBiotech	4030-05
α-Goat	HRP	SouthernBiotech	6460-05

Supplementary Table 2: Human Donor Information

Group	Donor ID	Age [years]	Sex
Young Group Median age: 32.5 years Females: 25%	Young_1	25	Male
	Young_2	33	Male
	Young_3	33	Female
	Young_4	32	Male
Old Group Median age: 71.0 years Females: 33%	Old_1	67	Female
	Old_2	55	Male
	Old_3	80	Male
	Old_4	63	Male
	Old_5	75	Female
	Old_6	72	Male
	Old_7	67	Male
	Old_8	79	Male
	Old_9	71	Female

Supplementary Table 3: Data from Figure 3D

GO Term	Description	p-value	FDR	Count	Genes
GO:0001932	regulation of protein phosphorylation	2,21E-05	1,16E-01	20	Cdkn1c, Btc, Bmp4, Timp3, Gas6, Pdgfd, Plc1, Tnfaip3, Ocln, Smpd3, Fzd5, Plcb1, Pde5a, Tlr1, Cdk5r1, Ankrd6, Ksr1, Slc11a1, Gpnmb, Camkk1
GO:0045860	positive regulation of protein kinase activity	2,42E-04	6,35E-01	11	Fzd5, Btc, Pde5a, Bmp4, Tlr1, Cdk5r1, Gas6, Ksr1, Slc11a1, Pdgfd, Camkk1
GO:0042325	regulation of phosphorylation	2,68E-04	4,69E-01	20	Cdkn1c, Btc, Bmp4, Timp3, Gas6, Pdgfd, Plc1, Tnfaip3, Ocln, Smpd3, Fzd5, Plcb1, Pde5a, Tlr1, Cdk5r1, Ankrd6, Ksr1, Slc11a1, Gpnmb, Camkk1
GO:0051347	positive regulation of transferase activity	2,76E-04	3,63E-01	11	Fzd5, Btc, Pde5a, Bmp4, Serinc5, Tlr1, Cdk5r1, Gas6, Ksr1, Slc11a1, Pdgfd
GO:0007167	enzyme linked receptor protein signaling pathway	3,32E-04	3,49E-01	10	Smpd3, Soga1, Btc, Plcb1, Bmp4, Megf8, Gucy2g, Cdk5r1, Gas6, Pdgfd
GO:0055085	transmembrane transport	3,98E-04	3,48E-01	26	Trpc1, Sort1, Scn11a, Ga6, Slc16a4, Slc6a19, Slc9a8, Hcn1, Slc23a3, Itpr1, Slc11a1, Rhd, Tmco3, Slc20a2, Slc39a12, Slc27a4, Slc39a13, Scn2a1, Slc30a10, Slc35f1, Slc7a2, Hpn, Alg10b, Abcc9, Alc25a30, Fkbp1b
GO:0045859	regulation of protein kinase activity	4,22E-04	3,17E-01	13	Cdkn1c, Btc, Bmp4, Gas6, Pdgfd, Tnfaip3, Fzd5, Pde5a, Tlr1, Cdk5r1, Ksr1, Slc11a1, Camkk1
GO:0032417	positive regulation of sodium:proton antiporter activity	4,44E-04	2,91E-01	2	Plcb1, Tesc
GO:0032415	regulation of sodium:proton antiporter activity	4,44E-04	2,59E-01	2	Plcb1, Tesc
GO:0001934	positive regulation of protein phosphorylation	4,86E-04	2,55E-01	13	Btc, Bmp4, Gas6, Pdgfd, Fzd5, Plcb1, Pde5a, Tlr1, Cdk5r1, Ksr1, Slc11a1, Ankrd6, Gpnmb
GO:0002682	regulation of immune system process	5,15E-04	2,46E-01	18	Cd276, Spta1, Bmp4, Gas6, Zbtb16, Spon2, Pdgfd, Tnfaip3, Smpd3, Fzd5, C1rl, Plcb1, Ddx60, Pde5a, Tesc, Tlr1, Slc11a1, Gpnmb
GO:1903555	regulation of tumor necrosis factor superfamily cytokine production	6,20E-04	2,71E-01	6	Fzd5, Tlr1, Gas6, Spon2, Tnfaip3, Gpnmb
GO:0032680	regulation of tumor necrosis factor production	6,20E-04	2,50E-01	6	Fzd5, Tlr1, Gas6, Spon2, Tnfaip3, Gpnmb
GO:0071229	cellular response to acid chemical	6,67E-04	2,50E-01	3	Plcb1, Tesc, Pdgfd
GO:0033674	positive regulation of kinase activity	6,69E-04	2,34E-01	11	Fzd5, Btc, Pde5a, Bmp4, Tlr1, Cdk5r1, Gas6, Ksr1, Slc11a1, Pdgfd, Camkk1
GO:0002691	regulation of cellular extravasation	9,62E-04	3,16E-01	2	Plcb1, Pdgfd
GO:2000437	regulation of monocyte extravasation	9,62E-04	2,97E-01	2	Plcb1, Pdgfd

Supplementary Table 4: Data from Figure 3E

Gene	log2ratio[YUvsYC]	-log10[pval_YU_vs_YC]
Ppm1j	8,352310604	3,05E-08
Eml6	7,71988933	2,25E-05
Ocln	6,200369776	0,000194095
Pdgfd	6,052335111	0,00047957
Trem1	-8,025885335	0,000957357
Bmp4	5,365593736	0,003397018
Cdk5r1	5,547283848	0,004245703
Hrh2	6,337566369	0,004527515
Trem3	-8,526148984	0,004642915
Tnfaip3	6,701040475	0,005705899
Hectd2	5,756077353	0,006327258
Plcl1	4,534163271	0,009474752
Gas6	4,744492158	0,012017658
Socs7	2,574613829	0,013011665
Fcgr2b	-5,91947358	0,017270032
Il11	4,293118372	0,017448841
Prkci	2,041038002	0,017461162
Ptpn11	1,379582604	0,021868096
Cebpa	-5,222329074	0,023681109
Hspb8	3,825562144	0,02407896
Prkcb	3,800626251	0,027301982
Irf8	-4,789833405	0,0276582
Zap70	2,450950392	0,033369023
Rhoc	3,737242818	0,03356817
Il4	-3,643321404	0,038134857
Ccr2	-6,631600505	0,040740731

Supplementary Table 5: Data from Figure 3G

Protein IDs	Protein names	Gene name	Mol. weight [kDa]	LOG2 (Ube2g1/ctr)
Bait protein				
P62254;D6RES1	Ubiquitin-conjugating enzyme E2 G1;Ubiquitin-conjugating e	Ube2g1	19,509	8,387606404
Significantly enriched proteins (SigB)				
A0A0A6YW67;E9Q9J0;E9Q5F6;Q5SX22	Ubiquitin-60S ribosomal protein L40;Ubiquitin;60S ribosoma	Uba52	8,7279	5,688760512
E0CYW8		Creb3	5,5726	6,660076799
Q8C8I3;E9PUG7;A0A0R4J298;Q61211	Eukaryotic translation initiation factor 2D	Eif2d	50,089	3,842720958
Q922H1	Protein arginine N-methyltransferase 3	Prmt3	59,902	4,34686287
Q9ES97	Reticulon-3	Rtn3	103,88	4,240909003
G5E902;Q8VEM8	Phosphate carrier protein, mitochondrial	Slc25a3	39,736	4,240909003
P56873	Sjoegren syndrome/scleroderma autoantigen 1 homolog	Sssca1	21,336	4,240909003
Q99KF1	Transmembrane emp24 domain-containing protein 9	Tmed9	27,127	4,240909003
Slightly enriched proteins (LOG2 (Ube2g1/ctr)>2)				
Q61696;P17879	Heat shock 70 kDa protein 1A;Heat shock 70 kDa protein 1B	Hspa1a	70,078	3,268238584
P16627	Heat shock 70 kDa protein 1-like	Hspa1l	70,636	2,311084
P17156	Heat shock-related 70 kDa protein 2	Hspa2	69,641	2,815526742
Q3U2G2;Q61316	Heat shock 70 kDa protein 4	Hspa4	94,208	2,440637893
A0A0N4SUH8;Q9QZ23	NFU1 iron-sulfur cluster scaffold homolog, mitochondrial	Nfu1	28,654	3,291648515
Q9DBU3	Serine/threonine-protein kinase RIO3	Riok3	58,704	4,014575907
P61982	14-3-3 protein gamma;14-3-3 protein gamma, N-terminally p	Ywhag	28,302	2,352143664
A0A1W2P6R9;A0A0R4J211;G5E825;Q9	Rho guanine nucleotide exchange factor 25	Arhgef25	64,116	2,03048796
Q9CQQ7;A0A0G2JGX3	ATP synthase F(0) complex subunit B1, mitochondrial	Atp5f1	28,948	2,567060961
A0A0R4IZW8;O88456;A0A0R4J1C2	Calpain small subunit 1	Capns1	28,406	2,179152842
Q62426	Cystatin-B	Cstb	11,045	2,777159627
Q8BH95	Enoyl-CoA hydratase, mitochondrial	Echs1	31,474	3,736075522
Q9DCM0	Persulfide dioxygenase ETHE1, mitochondrial	Ethe1	27,738	3,313081915
P19157;P46425	Glutathione S-transferase P 1;Glutathione S-transferase P 2	Gstp1	23,609	3,462575024
P00493	Hypoxanthine-guanine phosphoribosyltransferase	Hprt1	24,57	2,893240508
F6RJV6;Q9JJK2	LanC-like protein 2	Lancl2	49,742	3,042036104
A2A813;Q99LX0;A2A815;A2A817;A2A81	Protein DJ-1	Park7	18,474	2,307930944
Q8K183	Pyridoxal kinase	Pdxk	35,015	2,198238424
A0A1W2P6Q4;P12382	ATP-dependent 6-phosphofructokinase, liver type	Pfkl	7,088	2,225597656
P20108	Thioredoxin-dependent peroxide reductase, mitochondrial	Prdx3	28,127	3,772640024
P49722	Proteasome subunit alpha type-2	Psma2	25,926	3,8081003
P35235	Tyrosine-protein phosphatase non-receptor type 11	Ptpn11	68,46	2,075190725
Q8K2B3	Succinate dehydrogenase [ubiquinone] flavoprotein subunit,	Sdha	72,585	2,490640739
Q9CQA3	Succinate dehydrogenase [ubiquinone] iron-sulfur subunit, n	Sdhb	31,814	2,448896515
Q9QZD8	Mitochondrial dicarboxylate carrier	Slc25a10	31,715	2,753724829
A2AQU8;Q9D975	Sulfiredoxin;Sulfiredoxin-1	Srxn1	16,063	3,610604168
A0A1B0GR11;Q93092	Transaldolase	Taldo1	42,151	3,286025997
P17751;H7BXC3	Triosephosphate isomerase	Tpi1	32,191	3,035519396
D3Z6I8;E9Q7Q3;A0A0R4J1P2;P21107;I	Tropomyosin alpha-3 chain	Tpm3	28,723	2,425450645
P68510	14-3-3 protein eta	Ywhah	28,211	3,529074473